

GALACTIC MAGNETISM PHD STUDY GUIDE

Jessica Campbell, Dunlap Institute for Astronomy & Astrophysics (UofT)

Contents

1 Preface	1
2 Terminology	2
3 Variables	27
4 Equations	30

1 Preface

The interstellar medium (ISM) is a complex environment of gas and dust with varying degrees of ionization, densities, and spatial distributions called *phases*. It accounts for $\sim 10 - 15\%$ of the mass and 1 – 2% of the volume of our Galaxy. From the largest of Galactic scales to the smallest scales of star and planet formation, this tenuous plasma is threaded with magnetic field lines and exhibits large degrees of turbulence, both of which are believed to be major driving forces in shaping the structure and dynamics of our Galaxy. These magnetic fields, along with cosmic rays, exert outward pressures on the ISM which are counterbalanced by the gravitational attraction provided by the ordinary matter. The ordinary matter, cosmic rays, and magnetic fields are therefore in a state of pressure equilibrium. Turbulence is an important aspect of the ISM as it not only transports energy from large (\sim kpc) to small (\sim pc) scales, but also amplifies magnetic fields and accelerates cosmic rays, explaining the observed μ G magnetic field strengths as well as the \sim GeV cosmic ray energies in our Galaxy. Turbulence itself is a complex non-linear fluid phenomenon which results in an extreme range of correlated spatial and temporal scales in the multi-phase ISM, and is driven by a variety of large- and small-scale energy sources. While magnetic fields and turbulence are generally understood to play fundamental roles in shaping the structure and dynamics of our Galaxy, the degree to which they do so across different phases and spatial scales of the ISM remains poorly understood.

2 Terminology

Advection: The transport of a substance by bulk motion.

Advection operator:

Alfvén Mach number: A commonly used parameter of turbulence used to obtain information on gas compressibility and magnetization given by

$$\mathcal{M}_A \equiv \frac{|\vec{v}|}{v_A},$$

where $|\vec{v}|$ is the local velocity and v_A is the *Alfvén speed*.

Alfvén speed (v_A): Given by

$$v_A = \frac{|\vec{B}|}{4\pi\rho_n} [\text{m s}^{-1}],$$

where $|\vec{B}|$ is the magnetic field strength and ρ is the density of neutral particles. When the Alfvén speed is greater than the sound speed, the fast and Alfvén wave families are damped at or below the *ambipolar diffusion scale* L_{AD} ; when the Alfvén speed is less than the sound speed, the slow and Alfvén wave families are damped.

Alfvén wave: In 1942, Hannes Alfvén combined the mathematics of fluid mechanics and electromagnetism to predict that plasmas could support wave-like variation in the magnetic field, a wave phenomenon that now bears his name, Alfvén waves. These are a type of magnetohydrodynamic (MHD) wave in which ions oscillate in response to a restoring force provided by an effective tension on the magnetic field lines. The waves initially proposed by Alfvén are considered “basic”. They have a characteristic that they are compressional, which means that magnetic field variation of the Alfvén waves is in the direction of the wave motion. Charged particles moving through a plasma with these waves have very little alteration of their trajectory. But Alfvén waves can exhibit more variety. A variant is the “kinetic” Alfvén wave which is transverse, with strong magnetic field variation perpendicular to the wave motion, so can trade energy between the different frequencies which might propagate through a plasma. This also means it can exchange energy with the particles in the plasma, in some cases, trapping particles in the troughs of the waves and carrying them along.

Ambipolar diffusion: In many situations, ideal MHD is not a sufficiently good assumption and additional effects need to be accounted for. In many contexts, the dominant correction is the so-called ambipolar diffusion. Since the neutrals are not charged they are not subject to the *Lorentz force* which applies only on the ions. However, through collisions the neutrals and the ions exchange momentum and therefore the Lorentz force has an influence on the neutrals through the ions. If the number of ions is large (i.e., if the ionization is high) the number of collisions is expected to be large and ideal MHD remains a good approximation. However in regions like molecular clouds, the ionization is usually of the order of 10^{-7} and therefore the two fluids are not perfectly coupled. The ions drag the field lines and drift with respect to the neutrals implying that the latter can cross the field lines. The field is not frozen in the gas anymore. The drift of neutral particles towards the central gravitational potential through the ionized particles tied to the magnetic field. This is often invoked as a source of dissipation of the MHD energy cascade. The scale at which ions and neutral particles decouple is called the *ambipolar diffusion scale*. The application of ambipolar diffusion extends beyond direct studies of star formation and to include general studies of magnetic fields. Ambipolar diffusion has been proposed to damp particular families of MHD waves.

Ambipolar diffusion scale (L_{AD}): The scale at which ions and neutral particles decouple through the process of *ambipolar diffusion*. It can be estimated as the scale at which the *Reynolds number*, with diffusivity given by ambipolar diffusivity, is equal to unity. The ambipolar diffusion scale has been thought to set the dissipation scale of turbulence in molecular clouds and set a fundamental characteristic scale for gravitational collapse in star formation. When the Alfvén speed is greater than the sound speed, the fast and Alfvén wave families are damped at or below the *ambipolar diffusion scale* L_{AD} ; when the Alfvén speed is less than the sound speed, the slow and Alfvén wave families are damped. On scales larger than L_{AD} , it was also predicted that two-fluid turbulence (ion-neutral) acts like single-fluid MHD turbulence. The *ambipolar diffusivity* is given by

$$\nu_{AD} = \frac{B^2}{4\pi\rho_i\rho_n\alpha} [\text{m}^2 \text{s}^{-1}],$$

where ρ_i and ρ_n are the density of the ions and neutrals, respectively, B is the magnetic field strength, and α is the frictional coupling coefficient between the ions and neutrals. The *Reynolds number* for ion-neutral drift is defined as

$$R_{\text{AD}} = \frac{LV}{\nu_{\text{AD}}} \text{ [dimensionless]},$$

where V is a characteristic velocity (e.g., for trans-Alfvénic turbulence it is the *Alfvén speed*, $v_A = \frac{B}{4\pi\rho_n}$) and $L = L_{\text{AD}}$ when $R_{\text{AD}} = 1$. This gives the form of the ambipolar diffusion scale as often found in the literature:

$$L_{\text{AD}} = \frac{V_A}{\alpha\rho_i} \text{ [m].}$$

It has been shown that the plane-of-sky magnetic field can be estimated using the ambipolar diffusion length scale.

Autocorrelation: The correlation of a signal with a delayed copy of itself as a function of delay. Informally, it is the similarity between observations as a function of the time lag between them. The autocorrelation of an observable A with position r and position increment δr is given by

$$C(\delta r) = \langle f(r)f(r + \delta r) \rangle \text{ [dimensionless].}$$

Axi-symmetric spiral (ASS) model:

Azimuthal magnetic field (\vec{B}_θ): Often the Galactic magnetic field is expressed in cylindrical coordinates (θ, r, z) . The azimuthal component (\vec{B}_θ) dominates the Galactic disk where the radial (\vec{B}_r) and vertical (\vec{B}_z) components are generally weak.

Balbus-Hawley instability: See *magnetorotational instability*.

Bandwidth depolarization: A type of *external depolarization* where the polarization vector is substantially rotated within the observing bandwidth if the Faraday depth is large enough.

Beam depolarization: A type of *external depolarization* due to fluctuations in the foreground screen within the observing beam: unresolved density or magnetic field inhomogeneities of the media through which the radiation propagates induces unresolved spatial variations in the Faraday rotation measure.

Biermann battery mechanism: The process by which a weak seed magnetic field can be produced from zero magnetic field initial conditions via perpendicular density and temperature gradients. The Biermann mechanism can explain the generation of a $\sim 10^{-20}$ G field after recombination, but it is questionable whether turbulent dynamo growth alone can explain amplification up to the $10 \mu\text{G}$ fields seen today throughout the ISM. A possible solution to this problem may be provided by the potential role played by kinetic instabilities in the amplification of magnetic fields. One such instability is the *Weibel instability*. Temperature gradients form perpendicular to astrophysical shocks (hotter in the center of the shock), while density gradients form parallel to the shock, once again allowing the Biermann battery to take place. The Biermann mechanism is also the presumed cause of self-generated magnetic fields ($\sim 10^6$ G) found in laser-solid interaction experiments. The laser generates an expanding bubble of plasma by hitting and ionizing a solid foil of metal or plastic. This bubble thus has a temperature gradient perpendicular to the beam (hottest closest to the beam axis), and a density gradient in the direction normal to the foil, allowing for the Biermann battery mechanism to take place. Assuming a two-fluid description of a plasma with massless electrons, the magnetic field evolution is given by the generalized *induction equation*:

$$\frac{\partial \vec{B}}{\partial t} = \nabla \times (\vec{v} \times \vec{B}) + \frac{\eta c^2}{4\pi} \nabla^2 \vec{B} - \frac{1}{en} \nabla \times (\vec{j} \times \vec{B}) - \frac{c}{ne} \nabla n \times \nabla T_e,$$

which shows the evolution of magnetic field \vec{B} , based on the fluid velocity \vec{v} , the current density $\vec{j} = c\nabla \times \vec{B}/4\pi$, the number density n , and the electron temperature $T_e = P_e/n$, where P_e is the electron plasma pressure. Here, c is the speed of light, η is the resistivity, and e is the charge of an electron. The terms on the RHS from left to right are the convective term, the resistive term, the Hall term, and the Biermann battery term. Starting with $\vec{B} = 0$, all terms on the RHS except for the Biermann term can be ignored, and thus \vec{B} grows linearly. Based on scaling, given $T_e = m_e v_{\text{th}}^2$, we find

$$B(t) \approx \frac{m_e c}{e} \frac{v_{\text{th}}^2}{L_T L_n} t \text{ [G]},$$

where L is more precisely defined by the length of the gradients ($L_n \equiv n/\nabla n$, $L_T \equiv T_e/\nabla T_e$, which can be assumed to be approximately comparable).

Birefringence: The optical property of a medium to have a refractive index that is dependent on the polarization and direction of propagation of light. Birefringence implies that there are two natural wave modes which may be described by their polarizations, which are necessarily orthogonal to each other, and by Δk , the difference in their wavenumbers. The magnetoionic medium is an example of such a medium as the *polarization angle* of light becomes rotated as it propagates via Faraday rotation as a function of frequency.

Bi-symmetric spiral (BSS) model:**Bonnor-Ebert sphere:**

Bremmstrahlung radiation: Also known as “braking radiation”. This radiation is produced by the deceleration of a charged particle after being deflected by another charged particle, typically an electron by an atomic nucleus. The particle being deflected loses energy which is lost via radiation of a photon. For example, when free electrons within an H_{II} region pass near a positive ion (H⁺, He⁺) they are accelerated by the Coulomb field and emit bremsstrahlung radiation. Bremsstrahlung emission is a source of polarized continuum radiation and is a type of free-free radiation.

β parameter: The squared ratio of the sound speed to the Alfvén speed:

$$\beta \equiv \frac{c_s^2}{v_A^2} \text{ [dimensionless].}$$

Cascade rate:

Central molecular zone (CMZ): The inner ~ 500 pc of the Galaxy which contains $\lesssim 10\%$ of the MW’s molecular gas but $\sim 80\%$ of the dense ($n \gtrsim 10^3$ cm⁻³) gas: a reservoir of $2 - 6 \times 10^7 M_\odot$ of molecular material. The physical properties of the ISM in the CMZ differ substantially from those in the disc. Gas column and volume densities can be ~ 2 orders of magnitude greater, velocity dispersions measured for a given physical size are larger, and although there exists a significant fraction of cold dust, gas temperatures can range from 50 – 400 K.

Chandrasekhar-Fermi method: Originally proposed by Chandrasekhar & Fermi (1953) to estimate the field strength in spiral arms, the Chandrasekhar-Fermi method uses starlight polarization to estimate the average field strength $\langle B \rangle$ in a region. The method relates the line-of-sight velocity dispersion to the dispersion of starlight polarization angles about a mean component. Assuming that turbulence isotropically randomizes the magnetic field in the region, the mean field strength is given by

$$B_{\text{CF}}^2 \equiv \bar{B}^2 = \xi 4\pi \rho \frac{\sigma(v_{\text{los}})^2}{\sigma(\tan(\delta^*))^2},$$

where

$$\delta^* \equiv \theta^* - \bar{\theta}^*,$$

ρ is the gas density, θ^* is the mean starlight polarization angle, and ξ is a correction factor representing the ratio of turbulent magnetic to turbulent kinetic energy. The validity of the method depends critically on the presence of a significant mean field component.

Chaotic system:

Coherent magnetic field: See *ordered magnetic field*.

Cold neutral medium (CNM): A thermally-stable phase of the atomic ISM with a typical density and kinetic temperature of $n \sim 7 - 70$ cm⁻³ and $T_K \sim 60 - 260$ K, respectively. It seems almost certain that the CNM transitions to the DMM before transitioning to the classical MM. Our current knowledge of physical conditions and morphology in the CNM depends overwhelmingly on results from the Millennium survey of Heiles & Troland (2005), who used Arecibo with long integration times suitable for detecting Zeeman splitting. For the HI line in absorption, they derived column densities, temperatures, turbulent Mach number, and magnetic fields. HI CNM column densities are usually below 10²⁰ cm⁻² with a median value $N(\text{HI}) \sim 0.5 \times 10^{20}$ cm⁻². The median spin temperature is $T_s \sim 50$ K, median turbulent Mach number is $M_s \sim 3.7$, and median magnetic field is $\sim 6 \mu\text{G}$. By assuming reasonable values for the thermal gas pressure and comparing observed column densities, shapes and angular sizes as seen on the sky, Heiles & Troland (2003) find that interstellar CNM structures cannot be characterized as isotropic. The major argument is that a reasonable interstellar pressure, combined with the measured kinetic temperature, determines the volume density; this, combined with the observed column density, determines the thickness of the cloud along the line of sight. This dimension is almost always much smaller than the linear sizes inferred from the angular sizes seen on the sky. They characterize the typical structures as “blobby sheets”, which applies for angular scales of arcseconds to degrees.

It has been shown by numerical studies that CNM can be formed in a shock-compressed layer of the WNM.

Complex conjugate ($f(x)^*$ or $\bar{f}(x)$): The number with an equal real part and an imaginary part equal in magnitude but opposite in sign.

Compressible turbulence:

Compton scattering: The inelastic scattering of a photon by a free charged particle (usually an electron) in which energy is lost from the photon (typically a gamma ray or X-ray) which is in part transferred to recoiling the charged particle.

Cosmic rays: Extremely energetic and electrically charged particles pervading the ISM. The Galactic origin of the most energetic cosmic rays and their widespread distribution throughout the Milky Way

was not recognized until the observed Galactic radio emission was correctly identified with *synchrotron radiation* emitted by cosmic-ray electrons gyrating about the local Galactic magnetic field. Cosmic rays impinge on the ISM in three important ways: (1) they contribute to its ionization through direct collisions with gas particles, (2) they constitute a triple source of heating arising from the excess energy carried away by the electrons released in cosmic-ray ionization, from Coulomb encounters with charged particles of gas particles, and from the damping of Alfvén waves excited by cosmic rays streaming along magnetic field lines, and (3) they are dynamically coupled to the ISM via the magnetic field.

Dark molecular medium (DMM): Molecular gas in which hydrogen is molecular but the usual H₂ tracer, CO emission, is absent. Generally, the mass of DMM is found to be comparable to that of the CO-bright molecular medium (MM). It seems almost certain that the DMM is a transition state between the CNM and classical MM. Moreover, we expect the details of the DMM transition region to depend not only on physical conditions but also cloud morphology as it determines whether UV photons can penetrate to destroy molecules via photodissociation or photoionization. It seems very unlikely that one can understand the transition between atomic and molecular gas without understanding the effect of UV photons, and thus cloud morphology. In addition, there are hints that cloud morphology is affected by the magnetic field; after all, magnetic forces are one of the important forces on the ISM (the others being turbulent pressure, cosmic ray pressure (coupled to the gas by the magnetic field), thermal pressure, and gravity).

Delta variance ($\sigma_{\Delta}^2(L)$): A way to measure power on various scales defined as

$$\sigma_{\Delta}^2(L) = \left\langle \int_0^{3L/2} (A[r+x] - \langle A \rangle) \odot (x)^2 dx \right\rangle,$$

for a two-step function

$$\odot(x) = \pi \left(\frac{L}{2} \right)^{-2} \times \begin{cases} 1, & \text{if } x < (L/2) \\ -0.125, & \text{if } (L/2)x < (3L/2) \end{cases}.$$

The delta variance is related to the *power spectrum* $P(k)$: for an emission distribution with a power spectrum $P(k) \propto k^{-n}$ for wavenumber k , the delta variance is $\sigma_{\Delta}^2(L) \propto r^{n-2}$ for $r = 1/k$.

Depolarization: A reduction in the degree of polarization, measured as the ratio of the observed to the intrinsic polarization, either at a given frequency or when comparing two frequencies. Such depolarization can be caused by Faraday rotation in two different circumstances: *internal depolarization* or *external depolarization*. In order to distinguish between internal and external depolarization, very high resolution and sensitive polarization data at multiple frequencies are needed. The key difference is that internal depolarization should be correlated with the Faraday RM (such that regions with small RM exhibit low amounts of depolarization) whereas external depolarization should be correlated with the gradient of the RM.

Depolarization canals: Caused either by resolution-element or line-of-sight effects.

Depth depolarization:

Dispersion measure (DM):

$$DM = - \int_{\text{source}}^{\text{observer}} n_e d\vec{l} [\text{pc cm}^{-3}]$$

Dust polarization: The polarization angle of dust emission is conventionally taken to be 90° from the orientation of the local Galactic magnetic field.

Dynamo theory: The mechanism by which a magnetic field is produced in which a rotating, convecting, and electrically conducting fluid can generate and maintain a magnetic field over astronomical timescales. The dynamo that creates the large-scale magnetic field acts by violation of the reflection symmetry of the turbulence in rotating galaxies; this violation is associated, in turn, with dominance of, for example, right-handed helical motions in the turbulent flow.

Eddies:

Eddy interaction rate:

Emission measure (EM): The square of the number density of free electrons integrated over the volume of plasma.

$$EM = - \int_{\text{source}}^{\text{observer}} n_e^2 d\vec{l} [\text{pc cm}^{-6}]$$

Energy cascade:

Energy spectrum ($E(k)$): The term energy refers to any squared quantity, not necessarily velocity.

Epicycles: Small oscillations that Galactic disk stars experience about a perfectly circular orbit in the Galactic plane due to their velocity dispersion of $\sim 10 - 40 \text{ km s}^{-1}$ about their $\simeq 220 \text{ km s}^{-1}$ rotational velocity.

External depolarization: Depolarization induced by the limitations of the instrumental capabilities. For example, *beamwidth depolarization* is due to fluctuations in the foreground screen within the observing beam: unresolved density or magnetic field inhomogeneities of the media through which the radiation propagates induces unresolved spatial variations in the Faraday rotation measure. Another form of external depolarization is *bandwidth depolarization* which can occur when a significant rotation of the *polarization angle* is produced across the observing bandwidth.

Faraday depth (ϕ): The Faraday depth of a source is defined as

$$\phi(\mathbf{r}) = -0.81 \int_{\text{source}}^{\text{observer}} n_e \vec{B} \cdot d\vec{r} [\text{rad m}^{-2}],$$

where n_e is the electron density in cm^{-3} , \vec{B} is the magnetic field strength in μG , and $d\vec{r}$ is an infinitesimal path length in pc. The negative sign sets the convention that ϕ is positive for a B direction pointing towards the observer. Most compact sources like pulsars and extremely compact extragalactic sources show a single value of ϕ , called the *rotation measure* (RM). The Faraday depth (or RM) does not increase monotonically with distance along the line of sight.

Faraday dispersion: A type of *internal depolarization* caused by emission at different Faraday depths along the same line of sight.

Faraday dispersion function ($F(\phi)$): Also referred to as the *Faraday spectrum* introduced by Burn (1966) which describes the complex polarization vector as a function of Faraday depth as

$$F(\phi) = \int_{-\infty}^{\infty} P(\lambda^2) e^{-2i\phi\lambda^2} d\lambda^2 [\text{rad m}^{-2}],$$

where $F(\phi)$ is the complex polarized surface brightness per unit Faraday depth and $P(\lambda^2) = p(\lambda^2)I(\lambda^2)$ is the complex polarized surface brightness. To obtain the Faraday dispersion function, *rotation measure (RM) synthesis* is used to Fourier transform the observed polarized surface brightness into the Faraday spectrum. This Faraday dispersion function is not straightforward to interpret; in particular, there is no direct relationship between Faraday depth and physical depth. Further, the Faraday dispersion function suffers from sidelobes of the main components caused by limited coverage of the observed wavelength space. Burn (1966) assumes that $F(\phi)$ is independent of frequency. The equation for $P(\lambda^2)$ is very similar to a Fourier transform; a fundamental difference is that $P(\lambda^2)$ only has physical meaning for $\lambda \geq 0$. Since $P(\lambda^2)$ cannot be measured for $\lambda < 0$, it is only invertible if one makes assumptions about the values of P for $\lambda^2 < 0$ based on those for $\lambda^2 \geq 0$ (Burn 1966). For example, assuming that $P(\lambda^2)$ is Hermitian corresponds to assuming that $F(\phi)$ is strictly real.

Faraday rotation: A frequency-dependent magneto-optical phenomenon (i.e., an interaction between light and a magnetic field) in which the plane of polarization is rotated by an amount that is linearly proportional to the strength of the magnetic field in the direction of propagation. The Faraday effect is very useful in studies of galactic magnetism because it allows one to determine not only the strength but also the direction of a magnetic field. A linearly polarized electromagnetic wave propagating along the magnetic field of an ionized medium can be decomposed into two circularly polarized modes: a right-hand mode, whose \vec{E} vector rotates about the magnetic field in the same sense as the free electrons gyrate around it, and a left-hand mode, whose \vec{E} vector rotates in the opposite direction. As a result of the interaction between the \vec{E} vector and the free electrons, the right-hand mode travels faster than the left-hand mode; consequently the plane of linear polarization experiences Faraday rotation as the wave propagates. Faraday rotation results from the fact that right-handed circularly (RHC) and left-handed circularly (LHC) polarized light experience different phase velocities when traveling through a magnetoionic medium. Faraday rotation is induced by thermal electrons (not synchrotron radiation) coincident with a magnetic field which is at least partially oriented along the line of sight between the source and the observer. Non-thermal electrons have linear (not circular) modes, and produce *generalized Faraday rotation*. The Faraday rotation is used to measure the parallel component of the magnetic field via ionized gas. Given an initial polarization angle χ_0 and an observing frequency λ^2 , the observed polarization angle is a function of the Faraday depth ϕ of the medium at a given physical distance \mathbf{r} given by

$$\chi = \chi_0 + \phi(\mathbf{r})\lambda^2 [\text{rad}].$$

When a straight line is fit to this equation to provide a single value for $\phi(\mathbf{r})$, this is traditionally called the *rotation measure* (RM). This would only be a valid approximation for the simplest of cases, for example, a single foreground medium inducing Faraday rotation that is itself not emitting its own polarized emission. In more complex scenarios, polarized synchrotron emission may originate from volumes that are also inducing Faraday rotation which leads to polarized synchrotron emission at a range of Faraday depths. In such situations, *rotation measure synthesis* (RM-synthesis) must be done to obtain the Faraday depth as a function of physical distance, $\phi(\mathbf{r})$. The Faraday depth $\phi(\mathbf{r})$ is a proportionality constant that encapsulates the physics of the situation:

$$\phi(\mathbf{r}) = -0.81 \int_{\text{source}}^{\text{observer}} n_e \vec{B} \cdot \vec{r} [\text{rad m}^{-2}].$$

Additional complications may arise if the Faraday depth is large enough to substantially rotate the polarization vector within the observing bandwidth, an effect known as *bandwidth depolarization*.

Faraday spectrum: See *Faraday dispersion function*.

Faraday screen: A background emitting source of radiation which experiences Faraday rotation by a foreground source. In this case, and Faraday depth are identical; otherwise Rotation Measure Synthesis is needed.

Faraday thick: A source is Faraday thick if the wavelength squared times the extent of the object in units of Faraday depth is much greater than 1: $\lambda^2 \Delta\phi \gg 1$. In the case of Faraday thick, objects are extended in Faraday space and substantially depolarized at wavelength squared. Remember that whether an object is Faraday thin or Faraday thick is wavelength dependent.

Faraday thin: A source is Faraday thin if the wavelength squared times the extent of the object in units of Faraday depth is much less than 1: $\lambda^2 \Delta\phi \ll 1$. In the case of Faraday thin, objects are well approximated by a Dirac-delta function in Faraday space. Remember that whether an object is Faraday thin or Faraday thick is wavelength dependent.

Filling factor: See *volume filling factor*.

First moment: See *mean*.

Fluid turbulence:

Flux freezing: The coupling between the *cold neutral medium* (CNM) and the magnetic field due to its non-zero ionization fraction.

Forbidden line: Also known as a *forbidden mechanism* or a *forbidden transition*. A spectral line associated with the emission or absorption of light by atomic nuclei, atoms, or molecules which undergo a transition that is not allowed by a particular selection rule but does occur if the approximation associated with that rule is not made. Forbidden emission lines have been observed in extremely low-density gas and plasma in which collisions are infrequent. Under such conditions, once an atom or molecule has been excited for any reason into a meta-stable state, it is almost certain to decay by emission of a forbidden-line photon. Since meta-stable states are rather common, forbidden transitions account for a significant percentage of the photons emitted by the ultra-low density gas in space.

Fourier transform ($\hat{f}(x)$): Decomposes a function of time (a signal) into the frequencies that make it up. The Fourier transform (FT) of a function $f(x)$ is given by

$$\hat{f}(x) = \int_{-\infty}^{\infty} f(x') e^{-2\pi i x x'} dx'.$$

The reason for the negative sign convention in the definition of $\hat{f}(x)$ is that the integral produces the amplitude and phase of the function $f(x')e^{-2\pi i x x'}$ at frequency zero (0), which is identical to the amplitude and phase of the function $f(x')$ at frequency x' , which is what $\hat{f}(x)$ is supposed to represent. The function $f(x)$ can be reconstructed from its Fourier transform $\hat{f}(x)$, which is known as the Fourier inverse theorem.

Fourth moment: See *kurtosis*.

Fractional polarization ($p(\alpha)$):

Galactic magnetic field (GMF): Often the GMF is expressed in cylindrical coordinates (θ, r, z) . The *azimuthal magnetic field* (\vec{B}_θ) dominates the Galactic disk where the radial (\vec{B}_r) and vertical (\vec{B}_z) components are generally weak. The *toroidal magnetic field* refers to the structures (without \vec{B}_z components) confined to a plane parallel to the Galactic plane, while the *poloidal magnetic field* refers to the axisymmetric field structure around z (without \vec{B}_θ components) such as dipole fields. These terms are artificially designed for convenience when studying magnetic fields. Real magnetic fields would be all connected in space, with all components everywhere.

The RM sky is dominated by the GMF, with negligible contributions from the intergalactic medium and the RM intrinsic to the radio source (whether it be extragalactic radio sources or pulsars). A prominent

feature of the RM sky is the antisymmetry in the inner Galactic quadrants ($|\ell| < 90^\circ$). The positive RMs in the regions of ($0^\circ < \ell < 90^\circ, b > 0^\circ$) and ($270^\circ < \ell < 360^\circ, b < 0^\circ$) indicate that the magnetic fields point away from us. Such a high symmetry to the Galactic plane as the Galactic meridian through the Galactic center cannot simply be caused by localized features as previously thought. The antisymmetric pattern is very consistent with the magnetic field configuration of an *A0* dynamo, which provides such toroidal fields with reversed directions above and below the Galactic plane. The toroidal fields possibly extend to the inner Galaxy, even towards the *central molecular zone* (CMZ). This magnetic field model is also supported by the non-thermal radio filaments observed in the Galactic center region for a long time, which have been thought to be indications for the poloidal field in dipole form. The antisymmetric RM sky is also shown by pulsar RMs at high Galactic latitudes ($|b| > 8^\circ$). This implies that the magnetic field responsible for the antisymmetry pattern could be nearer than the pulsars.

Generalized Faraday rotation: In a medium whose natural modes are linearly or elliptically polarized, the counterpart of Faraday rotation, referred to as “generalized Faraday rotation”, can lead to a partial conversion of linear into circular polarization.

Great circle: A circle on the surface of a sphere that lies in a plane passing through the sphere’s center which represents the shortest distance between any two points on the surface of a sphere.

Gyration frequency (ω): The angular frequency of circular motion.

Hot ionized medium (HIM): Diffuse interstellar gas with a typical temperature of $T \sim 10^5 - 10^6$ K. This hot interstellar gas is believed to have been generated mainly by *supernovae* and stellar winds from massive stars, forming as the shock wave sweeps through the *interstellar medium*.

Hydrogen spectral series: Six named Hydrogen line series describing the emission spectrum of Hydrogen as dictated by the Rydberg equation. Includes the Lyman series ($n' = 1$), Balmer series ($n' = 2$), Paschen (or Bohr) series ($n' = 3$), Brackett series ($n' = 4$), Pfund series ($n' = 5$), Humphreys series ($n' = 6$).

HI fibers: Clark et al. (2014,2015) identified slender, linear HI features called “fibers” in the Galactic Arecibo L-Band Feed Array HI (GALFA-HI) survey data. By developing a new machine vision transformation technique named the *Rolling Hough Transform* (RHT), they identified the fibers and found that they are oriented along the interstellar magnetic fields probed by both starlight and dust polarization. They also showed that angular dispersion of the fibers can be used to measure the magnetic field strength through the *Chandrasekhar-Fermi method*. Based on the observed properties such as column density and line width, the HI fibers are suggested to be the CNM with density $\sim 10 \text{ cm}^{-3}$, temperature ~ 200 K, and width $\sim 0.1 \text{ pc}$ and are embedded in a shell of the local bubble. From the theoretical point of view, neither the origin of the HI fibers nor the mechanism of the alignment of the fibers and magnetic field is yet understood.

Using three-dimensional MHD simulations, Inoue & Inutsuka (2016) showed that shock sweeping of the magnetized WNM via supernova explosions creates thermally unstable gas in which fragmented HI clouds are formed as a consequence of the thermal instability. First, the shock compression creates a thermally unstable gas slab in which magnetic pressure balances upstream ram pressure. Then, the thermal instability develops to create the CNM in a cooling timescale of ~ 1 Myr. Because the timescale of the thermal instability that enhances gas density is governed by the cooling timescale, the thermal pressure is decreased down to the initial upstream level by the time of the CMN formation. This leads to the formation of a CNM with density $n \lesssim 100 \text{ cm}^{-3}$. If the initial magnetic field is in the same direction as the shock propagation, or if the magnetic field is neglected, the CNM forms at much higher densities. **H_{II} region:** The ionized clouds around massive OB stars which are responsible for ionizing most of the hydrogen around such stars. The boundaries of H_{II} regions are determined by the volume in which the rate of UV photoionization equals the rate of recombination of electrons. When free electrons within an H_{II} region pass near a positive ion (H⁺, He⁺) they are accelerated by the Coulomb field and emit radiation known as “free-free” or *bremssstrahlung emission* which is a source of polarized continuum emission. The average electron density of an H_{II} region is $\sim 10^3 \text{ cm}^{-3}$.

Ideal magnetohydrodynamics (MHD): Ideal MHD implies that fluid particles are attached to their field lines, that is to say they can flow along the field lines but cannot go across them. In a turbulent fluid, given the stochastic nature of the motions, such a situation would lead to a field that would be so tangled, that motions would quickly become prohibited. This implies that ideal MHD cannot, strictly speaking, be correct for a turbulent fluid and that some reconnection (i.e., some changes of the field lines topology) must be occurring. The physical origin of this reconnection is still debated but an appealing model has been proposed by Lazarian & Vishniac (1999). In this view the reconnection is driven by turbulence and is a multi-scale process, that is unrelated to the details of the microphysical processes. It is certainly the case, at least in numerical simulations of MHD turbulence, where the numerical diffusivity is often controlling the reconnection, that the MHD is far from being ideal. This process in particular induces an effective diffusion of the magnetic flux, that is therefore not fully frozen as one would expect if MHD was truly ideal.

Incompressible turbulence: The *Kolmogorov power spectrum* for incompressible turbulence in three dimensions is $P(k) \propto k^{-11/3}$ while its *energy spectrum* is $E(k) \propto k^{-5/3}$. In two dimensions, $P(k) \propto k^{-8/3}$ and $E(k) \propto k^{-5/3}$ (unchanged). For one dimension, $P(k) \propto k^{-5/3}$ and $E(k) \propto k^{-5/3}$ (unchanged).

Induction equation: Assuming a two-fluid description of a plasma with massless electrons, the magnetic field evolution is given by the generalized induction equation

$$\frac{\partial \vec{B}}{\partial t} = \nabla \times (\vec{v} \times \vec{B}) + \frac{\eta c^2}{4\pi} \nabla^2 \vec{B} - \frac{1}{en} \nabla \times (\vec{j} \times \vec{B}) - \frac{c}{ne} \nabla n \times \nabla T_e,$$

which shows the evolution of magnetic field \vec{B} , based on the fluid velocity \vec{v} , the current density $\vec{j} = c\nabla \times \vec{B}/4\pi$, the number density n , and the electron temperature $T_e = P_e/n$, where P_e is the electron plasma pressure. Here, c is the speed of light, η is the resistivity, and e is the charge of an electron. The terms on the RHS from left to right are the convective term, the resistive term, the Hall term, and the Biermann battery term. The induction equation is often simplified by assuming that the system size L is large compared to all kinetic scales, and only considering the convective term on the RHS.

Infrared polarization: The same large-scale alignment of aspherical, spinning dust grains that causes *starlight polarization* also causes polarization of far-infrared emission.

Intergalactic medium (IGM):

Internal depolarization: Depolarization due to the spatial extent of the source and occurs even if the intervening media are completely homogenous. Along the line of sight, the emission from individual electrons within a source arrive from different depths and suffer different Faraday rotation angles due to different path lengths. For the total radiation emitted by a source, this results in a reduction of the observed degree of polarization.

Interstellar medium (ISM): A tenuous medium throughout galaxies that consists of three basic constituents: (1) ordinary matter, (2) relativistic charged particles called cosmic rays, and (3) magnetic fields. These three basic constituents have comparable pressures and are bound together by electromagnetic forces. The ordinary matter itself consists of gas (atoms, molecules, ions, and electrons) and dust (tiny solid particles) which can exist in a number of phases: molecular, cold atomic, warm atomic, warm ionized, and hot ionized. Apart from the densest parts of molecular clouds whose degree of ionization is exceedingly low, virtually all interstellar regions are sufficiently ionized for their neutral component to remain tightly coupled to the charged component and hence to the local magnetic field. Cosmic rays and magnetic fields influence both the dynamics of the ordinary matter and its spatial distribution at all scales, providing, in particular, an efficient support mechanism against gravity. Conversely, the weight of the ordinary (i.e., baryonic) matter confines magnetic fields and, hence, cosmic rays to the Galaxy, while its turbulent motion can be held responsible for the amplification of magnetic fields and for the acceleration of cosmic rays. Studies of the diffuse ($n \sim 0.1 - 100 \text{ cm}^{-3}$) HI suggests that the magnetic field strength is relatively independent of its volume density, in contrast to magnetic fields in molecular clouds. The Galactic origin of the most energetic cosmic rays and their widespread distribution throughout the Milky Way was not recognized until the observed Galactic radio emission was correctly identified with *synchrotron radiation* emitted by cosmic-ray electrons gyrating about the local Galactic magnetic field. The ISM encloses but a small fraction of the total mass of the Galaxy. Moreover, it does not shine in the sky as visibly as stars do, yet it plays a vital role in many of the physical and chemical processes taking place in the Galactic ecosystem. The ISM is not merely a passive substrate within which stars evolve; it constitutes their direct partner in the Galactic ecosystem, continually exchanging matter and energy with them and controlling many of their properties. It is the spatial distribution of the ISM together with its thermal and chemical characteristics that determines where new stars form as well as their mass and luminosity spectra. These in turn govern the overall structure, optical appearance, and large-scale dynamics of our Galaxy. Hence understanding the present-day properties of our Galaxy and being able to predict its long-term evolution requires a good knowledge of the dynamics, energetics, and chemistry of the ISM. Table 1 outlines the different phases of the interstellar gas, including their typical temperature, number density, mass density, and total mass.

The MW is not a closed system. The evolution of the MW is significantly impacted by the two-way flow of gas and energy between the Galactic disk, halo, and IGM. We have long known that the atomic hydrogen halo extends far beyond the disk of the Galaxy. In recent years we have come to realize that the halo is also a highly structured and dynamic component of the Galaxy. Although we can now detect hundreds of clumped clouds in the atomic medium of the halo, we are far from understanding the halo's origin and its interaction with the disk of the Galaxy. It seems that a significant fraction of the structure of gas in the Galactic halo may be attributed to the outflow of structures formed in the disk, but extending into the halo. An example of such a structure may be an HI supershell. There are several examples of HI supershells that have grown large enough to effectively outgrow the Galactic HI disk. When this happens, the rapidly decreasing density of the Galactic halo does not provide sufficient resistance to the shell's expansion and it will expand unimpeded into the Galactic halo, creating a chimney from disk to

halo. These chimneys supply hot, metal-enriched gas to the Galactic halo and may act as a mechanism for spreading metals across the disk. It has been theorized that HI chimneys in the disk of the Galaxy may be a dominant source of structure for the halo through a Galactic Fountain model. Some Fountain models predict that cold cloudlets should develop out of the hot gas expelled by chimneys on timescales of tens of millions of years. Other Fountain theories suggest that the cool caps of an HI supershell will extend to large heights above the Galactic plane before they break. Once broken, the remains of the shell caps could be an alternate source of small clouds for the lower halo. Recent observational work has placed this theory on firmer footing, showing that the clumped clouds that populate the lower halo are not only more prevalent in regions of the Galaxy showing massive star formation than in less active regions, but that they extend higher into the halo in these regions.

Component	T (K)	n (cm^{-3})	Σ_{\odot} ($M_{\odot} \text{ pc}^{-2}$)	\mathcal{M} ($10^9 M_{\odot}$)
Molecular	10–20	10^2 – 10^6	~ 2.5	$\sim 1.3^{\text{a}}$ – 2.5^{b}
Cold atomic	50–100	20–50	~ 3.5	
Warm atomic	6000–10 000	0.2–0.5	~ 3.5	$\} \geq 6.0$
Warm ionized	~ 8000	0.2–0.5	~ 1.4	≥ 1.6
Hot ionized	$\sim 10^6$	~ 0.0065		

^aAdapted from Bronfman *et al.*, 1988.

^bAdapted from Clemens *et al.*, 1988.

Table 1: Descriptive parameters of the different components of the interstellar gas. T is the temperature, n is the true (as opposed to space-averaged) number density of hydrogen nuclei near the Sun, Σ_{\odot} is the azimuthally averaged mass density per unit area at the solar circle, and \mathcal{M} is the mass contained in the entire Milky Way. Both Σ_{\odot} and \mathcal{M} include 70.4% hydrogen, 28.1% helium, and 1.5% heavier elements. All values were rescaled to $R_{\odot} = 8.5 \text{ kpc}$. Table taken from Ferrière (2001).

Inverse Compton scattering: The upscattering of radio photons to become optical or X-ray photons by means of the inelastic scattering of a charged particle (usually an electron).

Inverse Fourier transform (IFT): The reconstruction of a function from its decomposition into the frequencies that make it up. The inverse Fourier transform (IFT) is given by

$$f(x) = \int_{-\infty}^{\infty} \hat{f}(x') e^{2\pi i x x'} dx'.$$

The fact that a function $f(x)$ can be reconstructed from its Fourier transform $\hat{f}(x)$ is known as the Fourier inverse theorem.

Kelvin-Helmholtz instability:

Kolmogorov microscale:

Kolmogorov spectrum:

Kurtosis: The fourth order statistical *moment* which is a measure of whether the data are heavy-tailed or light-tailed relative to a normal distribution. That is, data sets with high kurtosis tend to have heavy tails, or outliers. Data sets with low kurtosis tend to have light tails, or lack of outliers. Kurtosis is defined as

$$\text{Kurt}[x] = \frac{1}{N} \sum_{i=1}^N \left(\frac{x_i - \mu}{\sigma} \right)^3 \text{ [dimensionless]},$$

where μ is the statistical mean and σ is the standard deviation. Like the *skewness*, it is a dimensionless quantity.

Large scale magnetic field: How large is the “large” scale? Obviously it should be a scale, relatively much larger than some kind of standard. For example, the large-scale magnetic field of the Sun refers to the global scale field or the field with a scale length comparable to the size of the Sun, up to 10^9 m , rather than small-scale magnetic fields on the Solar surface. For the magnetic fields of our Galaxy, we should define the “large” scale as being a *scale larger than the separation between spiral arms*. That is to say, large scale means a scale larger than 2 – 3 kpc . Note that in the literature, “large” scale is sometimes used for large angular scale when discussing the structures or prominent plane-of-the-sky features (e.g., the large-scale features in radio continuum surveys). These large angular scale features are often very localized phenomena, and not very large in linear scale.

Lorentz factor (γ): The factor by which time, length, and relativistic mass change for an object while that object is moving with speed \mathbf{v} :

$$\gamma = \sqrt{\frac{1 - (v/c)^2}{c^2}}.$$

For non-relativistic motion $\gamma \approx 1$, while for relativistic motion $\gamma > 1$. For example, $\gamma(v = 0.9c) \approx 2$ and $\gamma(v = 0.99c) \approx 7$.

Lorentz force: The combination of electric and magnetic force on a point charge due to electromagnetic fields. A particle of mass m and charge q moving with a velocity v within a magnetic field \mathbf{B} experiences a force

$$\vec{F} = \frac{d}{d\tau}(m\gamma\vec{v}) = q \left(\vec{E} + \frac{\vec{v}}{c} \times \vec{B} \right) [\text{N}],$$

where τ is the retarded time and γ is the Lorentz factor. Of course, the Lorentz force only acts on charged particles but its effect is then transmitted to neutral particles via ion-neutral collisions.

Mach number:

Magnetic buoyancy: See Rayleigh-Taylor instability.

Magnetic reconnection:

Magnetohydrodynamic (MHD) equations: The equations of ideal MHD assume that the fluids are perfect conductors. The Lorentz force, which is the force that the EM fields \vec{E} and \vec{B} exert on the fluid must be taken into account. The EM field evolution is described by Maxwell equations. Written in CGS units, these equations are

$$\begin{aligned}\vec{\nabla} \cdot \vec{B} &= 0 \\ \vec{\nabla} \cdot \vec{E} &= 4\pi\rho_e \\ c\vec{\nabla} \times \vec{E} &= -\frac{\partial \vec{B}}{\partial t} \\ c\vec{\nabla} \times \vec{B} &= 4\pi\vec{j} + \frac{\partial \vec{E}}{\partial t},\end{aligned}$$

where ρ_e and \vec{j} are the fluid charge and current densities. The equation for charge conservation links these two quantities:

$$\frac{\partial \rho_e}{\partial t} + \vec{\nabla} \cdot \vec{j} = 0.$$

Magnetohydrodynamics (MHD): Magnetohydrodynamics (MHD) denotes the study of the dynamics of electrically conducting fluids. It establishes a coupling between the *Navier-Stokes equations* for fluid dynamics and Maxwell's equations for electromagnetism. The main concept behind MHD is that magnetic fields can induce currents in a moving conductive fluid, which in turn create forces on the fluid and influence the magnetic field itself.

Magnetoionic medium (MIM):

Magnetorotational instability: See Balbus-Hawley instability.

Meridian: A circle of constant longitude passing through a given place on Earth's surface and the terrestrial poles.

Microturbulence:

Milky Way Galaxy (MWG): We see the Milky Way as a narrow band encircling us because the Galaxy has the shape of a flattened disk within which we are deeply embedded. Our Galaxy comprises a thin disk with radius $\sim 25 - 30$ kpc and effective thickness $\sim 400 - 600$ pc, plus a spherical system itself composed of a bulge with radius $\sim 2 - 3$ kpc and a halo extending out to more than 30 kpc from the center. The Sun resides in the Galactic disk, approximately 15 pc from the midplane and 8.5 kpc away from the center. The stars belonging to the disk rotate around the Galactic center in nearly circular orbits. Their angular rotation rate is a decreasing function of their radial distance. At the Sun's orbital distance, the Galactic rotation velocity is $\simeq 220 \text{ km s}^{-1}$, corresponding to a rotational period of $\simeq 240 \times 10^6$ years. Disk stars also have a velocity dispersion of $\sim 10 - 40 \text{ km s}^{-1}$ which causes them to experience small oscillations about a perfectly circular orbit both in the Galactic plane (epicycles) and the vertical direction. In contrast, stars in the bulge and the halo rotate slowly and often have very eccentric orbits. Radio observations of interstellar neutral hydrogen indicate that the Milky Way possesses a spiral structure similar to those seen in optical wavelengths of external galaxies. The exact spiral structure of our own Galaxy is difficult to determine from within; the best radio data to date points to a structure characterized by a bulge of intermediate size and a moderate winding of the spiral arms. Infrared (IR) images of the Galactic center clearly display the distinctive signature of a bar. Our position in the spiral pattern can be derived from

local optical measurements which give quite an accurate outline of the three closest arms; they locate the Sun between the inner Sagittarius arm and the outer Perseus arm, near the inner edge of the local Orion-Cygnus arm.

Molecular medium (MM): Molecular gas is explored primarily with the 2.6 mm and other radio emission lines of the second most abundant molecule, CO, and secondarily with radio emission and absorption lines of less abundant molecules, such as OH, H₂O, and NH₃. Historically, molecular lines were seen mainly in emission towards the standard dense molecular clouds, and CO was emphasized to the extent that its presence *defined* molecular gas. While Spatially, the molecular gas is confined to discrete clouds, which are roundish, gravitationally bound, and organized hierarchically from large complexes (size $\sim 20 - 80$ pc and mass $\sim 10^5 - 10^6 M_{\odot}$) down to small clumps (size $\lesssim 0.5$ pc, mass $\lesssim 10^3 M_{\odot}$). Along the vertical direction, the molecular gas is the most strongly confined to the Galactic plane, with a HWHM thickness near the Sun $\sim 70 - 80$ pc. Horizontally, all the gas components tend to concentrate along the spiral arms, this tendency being probably most pronounced for the molecular gas. Upon averaging along Galactic circles, through spiral arms and interarm regions, it is found that most of the molecular gas resides in a ring extending radially between 3.5 – 7 kpc from the Galactic center. It seems almost certain that the DMM is a transition state between the CNM and classical MM. Moreover, we expect the details of the DMM transition region to depend not only on physical conditions but also cloud morphology as it determines whether UV photons can penetrate to destroy molecules via photodissociation or photoionization. It seems very unlikely that one can understand the transition between atomic and molecular gas without understanding the effect of UV photons, and thus cloud morphology. In addition, there are hints that cloud morphology is affected by the magnetic field; after all, magnetic forces are one of the important forces on the ISM (the others being turbulent pressure, cosmic ray pressure (coupled to the gas by the magnetic field), thermal pressure, and gravity).

nπ ambiguity: The inability to distinguish between polarization angles modulo π radians, rendering traditional linear RM fits often arbitrary. One way to deal with this ambiguity is to rely on resolving smooth spatial gradients in the polarization angle at each wavelength. With this assumption, the appropriate value of n can be resolved for each spatial pixel, yielding the correct polarization angle at each wavelength and thus the true value of RM. This is the basis of the PACERMAN routine developed by Dolag et al., (2005). However, routines like PACERMAN cannot deal with the second and third problems listed above since it is ultimately based on fitting a single value of RM along each line of sight.

Open cluster: A rather loose, irregular grouping of $10^2 - 10^3$ stars confined to the Galactic disk and therefore also known as Galactic clusters.

Ordered magnetic field: A.k.a. “coherent magnetic field”. Whether a magnetic field is ordered or random depends on the scales concerned. A uniform field at a 1 kpc scale could be part of random fields on a 10 kpc scale, while it is of a very large scale relative to the pc scale magnetic fields in molecular clouds. Uniform fields are ordered fields. Regularly ordered fields can coherently change their directions, so they may not be uniform fields.

Paramagnetism: Paramagnetic materials have unpaired electrons which, when in the presence of an external magnetic field such as the interstellar magnetic field, align in the same direction causing grain alignment.

Parker instability:

Passive mixing:

Pitch angle: The angle between a charged particle’s velocity vector and the local magnetic field.

Photodissociation region (PDR): Also known as *photon-dominated regions* or PDRs. Predominantly neutral regions of the ISM in which UV photons strongly influence the gas chemistry and act as the dominant energy source. They occur in any region of interstellar gas that is dense and cold enough to remain neutral, but that has too low of a column density to prevent penetration of far-UV photons from massive stars. They are also associated with HII regions. All of the atomic gas and most of the molecular gas is found in photodissociation regions.

Photon-dominated region (PDR): See *photodissociation region*.

Pitch angle: The angle between a charged particle’s velocity vector and the local magnetic field.

Plasma beta (β): The ratio of the gas to magnetic pressure. For either high or low β , it was predicted that *Alfvén waves* should damp at the *ambipolar diffusion scale* L_{AD} and thus the magnetohydrodynamic (MHD) cascade should damp past the ambipolar diffusion scale.

Poincaré sphere:

Polarized intensity (P): A measure of the total linear polarization in radio emission given as

$$P \equiv \sqrt{Q^2 + U^2} [\text{Jy}],$$

where Q is the *Stokes Q* polarization and U the *Stokes U* polarization. The images of P (as well as Q and U) are often filled with complex structures that bear little resemblance to the *Stokes I* image of total

intensity. The intensity variations seen in P (as well as Q and U) are the result of small-scale angular structure in the *Faraday rotation* induced by ionized gas, and are thus an indirect representation of turbulent fluctuations in the free-electron density and magnetic field throughout the *interstellar medium*. While Q and U exhibit Gaussian noise properties, this is not true for P . The noise in Q and U is squared when calculating P , having a Ricean distribution, and this causes the observed polarization intensity to be biased toward larger values.

Polarization angle (χ): Given by

$$\chi \equiv \frac{1}{2} \arctan \left(\frac{U}{Q} \right) [\text{rad}],$$

where Q is the *Stokes Q* polarization vector and U the *Stokes U* polarization vector. The arctan2 function is generally used to determine χ over the full $\pm n\pi$ range. The polarization angle (likewise with the amplitude of *polarized intensity*) is not preserved under arbitrary rotations and translations of the $Q-U$ plane. In the most general case, then, the observed values of χ (and $\mathbf{P} \equiv \sqrt{Q^2 + U^2}$) do not have any physical significance; only measurements of quantities that are both rotationally and translationally invariant in the $Q - U$ plane can provide insight into the physical conditions that produce the observed polarization distribution.

Polarization fraction ($p(\lambda^2)$):

$$p(\lambda^2) = \frac{P(\lambda^2)}{I(\lambda^2)} \text{ [dimensionless]},$$

where $P(\lambda^2)$ is the polarized surface brightness and $I(\lambda^2)$ is the total surface brightness.

Polarization gradient ($|\vec{\nabla} \vec{P}|$): The rate at which the *polarized intensity* complex vector $\vec{P} \equiv \sqrt{Q^2 + U^2}$ traces out a trajectory in the $Q-U$ plane as a function of position on the sky given by

$$|\vec{\nabla} \vec{P}| = \sqrt{\left(\frac{\partial Q}{\partial x} \right)^2 + \left(\frac{\partial U}{\partial x} \right)^2 + \left(\frac{\partial Q}{\partial y} \right)^2 + \left(\frac{\partial U}{\partial y} \right)^2} [\text{Jy beam}^{-1}],$$

or

$$\left| \frac{\partial \vec{P}}{\partial s} \right|_{\max} = \sqrt{\frac{1}{2} \left[\left(\frac{\partial Q}{\partial x} \right)^2 + \left(\frac{\partial U}{\partial x} \right)^2 + \left(\frac{\partial U}{\partial x} \right)^2 + \left(\frac{\partial U}{\partial y} \right)^2 \right] + \frac{1}{2} \sqrt{\left[\left(\frac{\partial Q}{\partial x} \right)^2 + \left(\frac{\partial U}{\partial x} \right)^2 + \left(\frac{\partial U}{\partial x} \right)^2 + \left(\frac{\partial U}{\partial y} \right)^2 \right]^2 - 4 \left[\frac{\partial Q}{\partial x} \frac{\partial U}{\partial y} - \frac{\partial Q}{\partial y} \frac{\partial U}{\partial x} \right]^2}},$$

where Q and U are the complex *Stokes vectors* and x and y are the Cartesian axes of the image plane. Note that $|\vec{\nabla} \vec{P}|$ cannot be constructed from the scalar quantity $P \equiv \sqrt{Q^2 + U^2}$, but is derived from the vector field $\vec{P} \equiv (Q, U)$. The amplitude of the polarization gradient $|\vec{\nabla} \vec{P}|$ provides an image of magnetized turbulence in diffuse, ionized gas manifested as a complex filamentary web of discontinuities in gas density and magnetic field strength. This quantity is rotationally and translationally invariant in the $Q - U$ plane, and so has the potential to reveal properties of the polarized distribution that might otherwise be hidden by excess foreground emission or *Faraday rotation*, or in data sets from which large-scale structure is missing. The polarization gradient is shown in Figure 1.

Using polarization gradients of isothermal MHD turbulence, the supersonic case (Figure 2c) was found to show localized groupings of very high-gradient filaments, corresponding to ensembles of intersecting shocks. By contrast, the subsonic (Figure 2a) and trans-sonic (Figure 2b) cases showed more diffuse networks of filaments, representing the cusps and discontinuities characteristic of any turbulent velocity field.

In the ISM, fluctuations in density and magnetic field will occur as a result of MHD turbulence, which will be visible in polarimetric maps. In the case of taking gradients of a turbulent field, one would expect to find filamentary structure created by shock fronts, jumps, and discontinuities. Figure 3 shows a schematic illustrating these three separate cases of a possible profile and its respective derivative. The cases are as follows:

- A Hölder continuous profile that is not differentiable at a given point (e.g., the absolute value function at the origin): common for all types of MHD turbulence. It is known that the turbulent velocity field in a Kolmogorov-type inertial range both in hydro and MHD is not differentiable, but only Hölder continuous. This case can be found in both subsonic- and supersonic turbulence.
- A jump profile: weak shocks, strong fluctuations, or edges (e.g., a cloud in the foreground which suddenly stops). This case creates a structure in the gradient by a shock jump or a large fluctuation

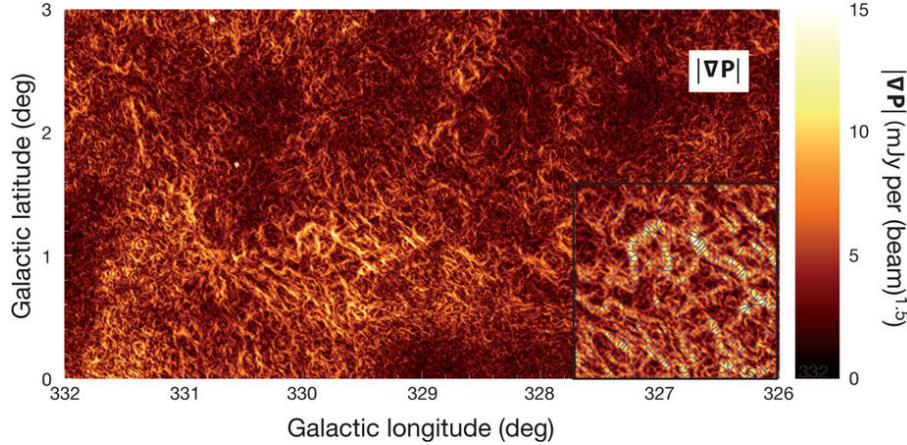


Figure 1: $|\vec{\nabla}\vec{P}|$ for an 18-deg² region of the Southern Galactic Plane Survey which reveals a complex network of tangled filaments. In particular, all regions in which $|\nabla\vec{P}|$ is high consists of elongated, narrow structures rather than extended patches. In the inset, the direction of $|\nabla\mathbf{P}|$ is shown for a small subregion of the image, demonstrating that $|\nabla\vec{P}|$ changes most rapidly along directions oriented perpendicular to the filaments. Figure taken from Gaensler (2011).

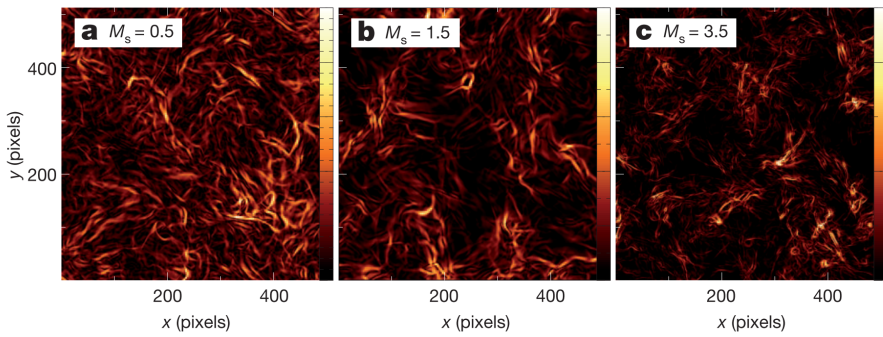


Figure 2: $|\vec{\nabla}\vec{P}|$ derived from propagation of linear radio polarization through three different isothermal simulations of magnetized turbulence. Figure taken from Gaensler (2011).

in either n_e or \vec{B} . Here again, this type of enhancement in $|\nabla\vec{P}|$ could be found in supersonic- and subsonic turbulence, and is due either to large random spatial increases or decreases due to turbulent fluctuations along the LOS or weak shocks. We expect weak shock turbulence to show a larger amplitude in $|\nabla\vec{P}|$ than the subsonic case due to increases in density fluctuations.

- A spike profile (e.g., delta function): strong shock regime. This case is unique to supersonic turbulence in that it represents a very sharp spike in n_e and/or \vec{B} across a shock front. The difference between this case and what might be seen in case two is that here we are dealing with interactions of strong shock fronts, which are known to create delta function-like distributions in density, creating a “double jump” profile across the shock front.

Of great interest is the question of which quantity is providing the dominant contribution to the structures in $|\nabla\vec{P}|$: $|\nabla n_{e,\text{LOS}}|$, $|\nabla \vec{B}_{\text{LOS}}|$, or both equally? Especially in the case of compressible turbulence, the magnetic energy is correlated with density: denser regions contain stronger magnetic fields due to the compressibility of the gas and the potential dynamo amplification of the magnetic field in dense gas. This causes the magnetic field to follow the flow of plasma if the magnetic tension is negligible. The compressed regions are dense enough to distort the magnetic field lines, enhance the magnetic field intensity, and effectively trap the magnetic energy due to the frozen-in condition. Thus, for the supersonic cases, the intensity of the structures seen in $|\nabla\vec{P}|$ is more pronounced than in the subsonic case. However, in the case of subsonic turbulence, there are no compressive motions. In this case, random fluctuations in density and magnetic field will create structures in $|\nabla\vec{P}|$. It's been shown using MHD simulations that in the case of subsonic turbulence, $|\nabla\vec{P}|$ correlates with $|\nabla\vec{B}|$ while in the supersonic case $|\nabla\vec{P}|$ correlates with density fluctuations. This is because density enhancements are dominant due to shock fronts in the case of supersonic turbulence, while in subsonic turbulence density is marginally incompressible.

Polarization gradient (radial component): The radial component quantifies how changes in polar-

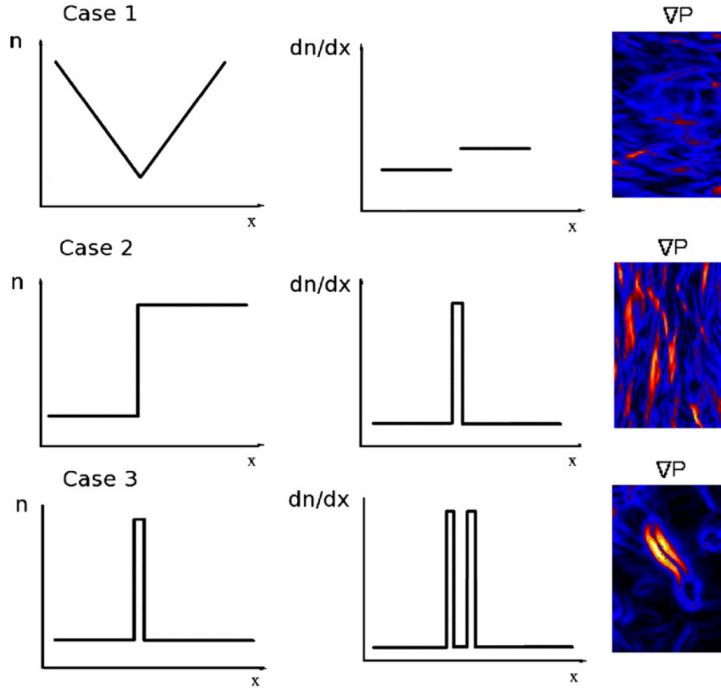


Figure 3: Schematic example of three possible scenarios for enhancements in a generic image “n,” where “n” could be $|\vec{P}|$, RM, or $\rho/N/\text{EM}$ (density, column density, emission measure). Case one (top row) shows an example of a Hölder continuous function that is not differentiable at the origin (applicable to all turbulent fields). Case two (middle row) shows an example of a jump resulting from strong turbulent fluctuations along the LOS or weak shocks. Case three (bottom row) shows a delta function profile resulting from interactions of strong shocks. In this case, the derivative gives a double jump profile which produces morphology that is distinctly different from the previous cases. In all cases we show examples from $|\vec{P}|$ simulations. Figure taken from Burkhart (2012).

ization intensity contribute to the directional derivative $|\partial \vec{P} / \partial s|$:

$$\left| \frac{\partial \vec{P}}{\partial s} \right|_{\text{rad}} = \sqrt{\frac{(Q \frac{\partial Q}{\partial x} + U \frac{\partial U}{\partial x})^2 + (Q \frac{\partial Q}{\partial y} + U \frac{\partial U}{\partial y})^2}{Q^2 + U^2}} [\text{Jy pc}^{-1}]$$

If changes in polarization intensity are dominant for a feature, then this could imply that the amount of depolarization due to the addition of polarization vectors along the line of sight varies significantly between different positions, and it follows that the medium producing the polarized emission may be very turbulent. This is true for both thermal dust emission and for synchrotron emission.

Polarization gradient (tangential component): The tangential component quantifies how changes in polarization angle, weighted by polarization intensity, contribute to the directional derivative $|\partial \vec{P} / \partial s|$:

$$\left| \frac{\partial \vec{P}}{\partial s} \right|_{\tan} = \sqrt{\frac{(Q \frac{\partial U}{\partial x} - U \frac{\partial Q}{\partial x})^2 + (Q \frac{\partial U}{\partial y} - U \frac{\partial Q}{\partial y})^2}{Q^2 + U^2}} [\text{Jy pc}^{-1}]$$

If changes in polarization angle are dominant, then this could indicate changes in the regular magnetic field threading the observed region, as this would produce significant changes in the emitted polarization angle in the case of thermal dust emission or synchrotron emission. Additionally, changes in the regular magnetic field may also cause the amount of Faraday rotation along different lines of sight to vary significantly, in the case of synchrotron emission.

Polarization gradient direction ($\arg \vec{\nabla} \vec{P}$): The direction of the *polarization gradient* at a given spatial position defined as

$$\arg(\vec{\nabla} \vec{P}) \equiv \arctan \left[\text{sign} \left(\frac{\partial Q}{\partial x} \frac{\partial Q}{\partial y} + \frac{\partial U}{\partial x} \frac{\partial U}{\partial y} \right) \frac{\sqrt{\left(\frac{\partial Q}{\partial y} \right)^2 + \left(\frac{\partial U}{\partial y} \right)^2}}{\sqrt{\left(\frac{\partial Q}{\partial x} \right)^2 + \left(\frac{\partial U}{\partial x} \right)^2}} \right] [\text{rad}],$$

where Q and U are the complex *Stokes vectors*.

Polarization horizon: The furthest distance we can see diffuse polarized emission.

Polarized surface brightness ($P(\lambda^2)$):

$$P(\lambda^2) = p(\lambda^2)I(\lambda^2) = Q + iU \text{ [Jy]},$$

where $p(\lambda^2)$ is the polarization fraction, $I(\lambda)$ is the total surface brightness, and Q and U are the complex Stokes vectors. The absolute value of this complex vector is given by

$$\|P(\lambda^2)\| = \sqrt{Q^2 + U^2} \text{ [Jy]},$$

where Q and U are the complex Stokes vectors.

Poloidal magnetic field: Often the GMF is expressed in cylindrical coordinates (θ, r, z) . The *poloidal magnetic field* refers to the axisymmetrical field structure around z (without \vec{B}_θ components) such as dipole fields.

Power spectrum ($P(k)$): Describes the distribution of power into frequency components composing that signal defined as

$$P(k) = \hat{f}(k)\hat{f}(k)^*,$$

for wavenumber k where $\hat{f}(k)$ denotes the *Fourier transform* (FT) and $\hat{f}(k)$ its *complex conjugate*. The power spectrum is the *Fourier transform* (FT) of the *autocorrelation function*.

Prandtl number: The ratio of momentum diffusivity (kinematic viscosity) to thermal diffusivity:

$$\text{Pr} = \frac{\nu}{\alpha} = \frac{\mu c_p}{k} \text{ [dimensionless]},$$

where $\nu = \mu/\rho$ is the momentum diffusivity (kinematic viscosity) in $\text{m}^2 \text{s}^{-1}$, $\alpha = k/(c_p\rho)$ is the thermal diffusivity in $\text{m}^2 \text{s}^{-1}$, μ is the dynamic viscosity in Pa s , k is the thermal conductivity in $\text{W m}^{-1} \text{K}$, c_p is the specific heat in $\text{J kg}^{-1} \text{K}$, and ρ is the density in kg m^{-3} .

$Q - U$ plane: Translations and rotations within the $Q - U$ plane can result from one or more of a smooth distribution of intervening polarized emission, a uniform screen of foreground *Faraday rotation*, and the effects of missing large-scale structure in an interferometric data set.

Random magnetic field: See *turbulent magnetic field*.

Rayleigh-Taylor instability: Also known as magnetic buoyancy.

Reynolds number (Re): An important dimensionless quantity in fluid mechanics used to help predict flow patterns in different fluid flow situations which characterizes the relative importance of inertial (resistant to change or motion) and viscous (heavy and gluey) forces:

$$\text{Re} = \frac{\rho v L}{\mu} \text{ [dimensionless]},$$

where ρ is the density in kg m^{-3} , v is the velocity in m s^{-1} , L is the characteristic length in m , and μ is the dynamic viscosity coefficient in Pa s . At low Reynolds numbers, flows tend to be dominated by laminar (sheet-like) flow, while at high Reynolds numbers, turbulence results from differences in the fluid's speed and direction, which may sometimes intersect or even move counter to the overall direction of the flow (eddy currents).

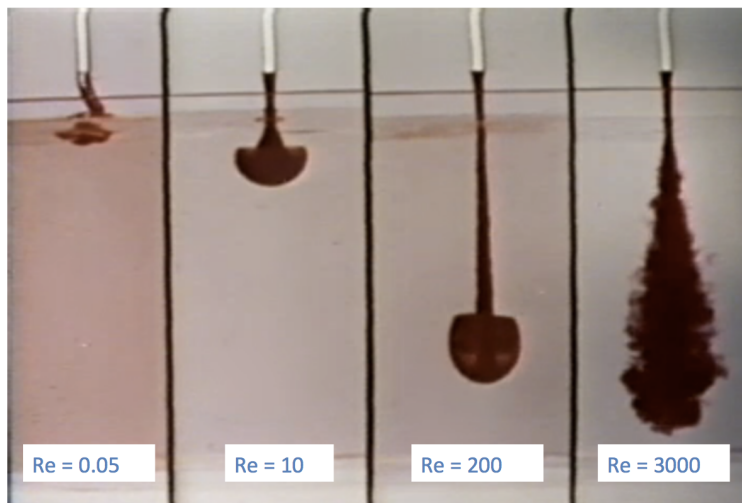


Figure 4: Flows at varying Reynolds number Re . In each panel, a fluid that has been dyed red is injected from the top into the clear fluid on the bottom. The fluids are glycerin-water mixture, for which the viscosity can be changed by altering the glycerin to water ratio. By changing the viscosity and the injection speed, it is possible to alter the Reynolds number of the injected flow. The frames show how the flow develops as the Reynolds number is varied. This image is a still from the National Committee for Fluid Mechanics Film series (Taylor, 1964), which, once you get past the distinctly 1960s production values, are a wonderful resource for everything related to fluids.

Rolling Hough Transform (RHT): A machine vision algorithm designed for detecting and parameterizing linear structure in astronomical data, originally applied to HI images. The detection of astronomical linear structure is approached in various ways depending on the context. Because HI structures are not objects with distinct boundaries, the problem is fundamentally different from many others. As these diffuse HI fibers were not formed by gravitational forces, there is no reason to require that they must be, or bridge, local overdensities. Indeed, these fibers are found often to be in groups of parallel structures, very unlike the cosmic web. Thus, methods developed for gravitationally dominated systems are not optimal for these purposes. The RHT is, as its name suggests, a modification of the Hough transform. The Hough transform was first introduced in a patent for the detection of complex patterns in bubble chamber photographs. It was soon recognized as a powerful line detection technique, and has found wide applications in image processing and machine vision. The adaption of the Hough transform with the RHT is a rolling version that is particularly well suited to the detection and quantization of specific linear features in astronomical data. The RHT does not merely identify fibers; it encodes the probability that any given image pixel is part of a coherent linear structure. This allows the user to quantify the linearity of regions of sky without specifying fibers as discrete entities. The RHT operates on two-dimensional data and is designed to be sensitive to linear structure irrespective of the overall brightness of the region. The first step is to unsharp mask the image. The image is convolved with a two-dimensional top-hat smoothing kernel of a user-defined diameter, D_K . The smoothed data is then subtracted from the original data and the resulting map is thresholded at 0 to obtain a bitmask. The subtraction of the smoothed component can be considered a suppression of large-scale structure, or a high-pass Fourier filter. Each straight line is parameterized in terms of the angle θ of its normal, and its minimum Euclidean distance from the origin ρ ,

$$\rho = x \cos \theta + y \sin \theta \text{ [pixels].}$$

Every possible line in the image space is uniquely specified by a point in the $\rho - \theta$ space. The RHT mapping is performed on a circular domain, diameter D_W , centered on each image-space pixel (x_0, y_0) in turn. Then a Hough transform is performed on this area, limited to $\rho = 0$. Thus the $\rho - \theta$ space is reduced to a one-dimensional space on θ for each pixel. All intensity over a set intensity threshold Z is stored as $R(\theta, x_0, y_0)$: RHT intensity as a function of θ for that pixel. Z is a percentage. In every direction θ , $Z \times D_W$ pixels must contain signal in order for the transform to record the data in that direction. We use the canonical binning for the number of theta bins:

$$n_\theta = \left[\pi \frac{\sqrt{2}}{2} (D_W - 1) \right] \text{ [dimensionless].}$$

By iterating (“rolling”) over the entire image space we produce the RHT output, $R(\theta, x, y)$. A visualization of the linear structures identified by the RHT, the **backprojection** $R(x, y)$, is obtained by integrating $R(\theta, x, y)$ over θ :

$$R(x, y) = \int R(\theta, x, y) d\theta \text{ [dimensionless].}$$

One advantage of the RHT is that the input parameters of the transform can be chosen to highlight specific linear features of interest. One defines, for a given run of the RHT, a smoothing kernel diameter (D_K), a window diameter (D_W), and an intensity threshold (Z). The rolling nature of the RHT ensures that linear structure at least as long as D_W will be identified. Thus D_W , along with the Z , sets a lower limit for the spatial length of the linear features. Thresholding below 100% ($Z < 1$) reflects the fact that structures can be physically coherent even if they are not visibly connected. $R(\theta, x, y)$ is intensity as a function of angle on a domain $\theta \in [0, \pi]$, as a 0° orientation is equivalent to a 180° orientation. $R(\theta, x, y)$ can be sampled in a circular region around each star in the field as

$$R_*(x, y) = \int \int_{\text{disk}} R(\theta, x, y) dx dy \text{ [dimensionless].}$$

To estimate the direction of a given region of the backrprojection $R_*(\theta, x, y)$, the expectation value is given by

$$\langle \theta \rangle' = \frac{1}{2} \arctan \left[\frac{\int \sin(2\theta) R_*(\theta) d\theta}{\int \cos(2\theta) R_*(\theta) d\theta} \right] \text{ [rad]}$$

where the equivalent value is found on the interval $\theta \in [0, \pi)$ via

$$\langle \theta \rangle = \pi - \text{mod}(\langle \theta \rangle' + \pi, \pi) \text{ [rad].}$$

Linear polarization data can be fully described by either a polarization angle χ and polarized intensity

P or by the Stokes parameters Q and U , where $\chi = (1/2) \arctan(U/Q)$ and $P = \sqrt{Q^2 + U^2}$. From the RHT output, similar ‘Stokes vectors’ can be defined via

$$Q_{\text{RHT}} = \int \cos(2\theta) R(\theta) d\theta \text{ [Jy]}$$

$$U_{\text{RHT}} = \int \sin(2\theta) R(\theta) d\theta \text{ [Jy].}$$

This allows for an estimate of the orientation of the magnetic field to be derived solely from HI data via

$$\theta_{\text{RHT}} = \frac{1}{2} \arctan \left(\frac{U_{\text{RHT}}}{Q_{\text{RHT}}} \right) \text{ [rad].}$$

Rotation measure (RM): Characterizes the amount of *Faraday rotation* that polarized light experiences while passing through thermal electrons. Most compact polarized sources like pulsars and extremely compact extragalactic sources show a single value of Faraday rotation which is the RM. This is commonly defined as the slope of the polarization angle χ versus λ^2 plot:

$$\text{RM} = \frac{d\chi(\lambda^2)}{d\lambda^2} \text{ [rad m}^{-2}\text{]},$$

where

$$\chi = \frac{1}{2} \arctan \left(\frac{U}{Q} \right) \text{ [rad].}$$

The RM, then, modifies the polarization angle χ from its initial value χ_0 as

$$\chi = \chi_0 + \text{RM} \lambda^2 \text{ [rad].}$$

The value of RM is the integral of the line-of-sight component of the magnetic field weighted by the line-of-sight distribution of electron density, given by

$$\text{RM} = -0.81 \int_{\text{source}}^{\text{observer}} n_e \vec{B} \cdot d\vec{l} \text{ [rad m}^{-2}\text{]},$$

where \vec{B} has units of μG , n_e has cm^{-3} , and $d\vec{l}$ has pc. The RM can be measured towards distant extragalactic radio sources and pulsars. The RM of an extragalactic radio source consists of an RM contribution intrinsic to the source, the RM from the intergalactic space from the source to the Galaxy, and the RM within the Galaxy. The first term (i.e., the extragalactic radio source) should be random and hence reasonably small on average, because a source can be randomly oriented in space with any possible field configuration; thus we observe a random quantity. The second term (i.e., the intergalactic source) is negligible on average. Intergalactic magnetic fields are too weak to be detected with current technology. Even if there is a weak field in intergalactic space, an integration over the path-length of the intergalactic magnetic field with random directions with extremely thin gas should give quite a small contribution. Therefore, the common contribution of RMs of extragalactic radio sources is from our own Galaxy.

The RM does not increase monotonically with distance along the line of sight. Traditionally, the RM is obtained by performing a least-squares fit to the data to determine the slope. There are however three potential problems to this method: (1) the observed polarization angle is only known modulo π radians; thus with measurements in only a few wavelength bands, the RM is often ambiguous (known as the *nπ ambiguity*), (2) polarized emission with different RM values can be present along a single line of sight; the signal from these regions mix, making a single linear fit inappropriate, and (3) faint sources with high RM will be undetectable in individual channels due to low signal to noise and will remain undetectable even after integrating all channels due to *bandwidth depolarization*; thus, no $\chi(\lambda^2)$ data will be available for the traditional linear fit.

Rotation measure (RM) synthesis: A robust method for determining the *Faraday dispersion function* as proposed by Burn (1966). It was seldom used until Brentjens and de Bruyn (2005) who coined the term *RM Synthesis*. This technique involves Fourier transforming the observed *polarized surface brightness* $P(\lambda^2)$ into the *Faraday dispersion function* $F(\phi)$ (also referred to as the *Faraday spectrum*) which is the complex polarized surface brightness as a function of *Faraday depth*. As shown by Burn (1966), the observed complex polarization vector can be written as $P(\lambda^2) = pIe^{2i\chi}$, where p is the *polarization fraction* and I is the *Stokes I* vector. Substituting the expression $\chi(\lambda^2) = \chi_0 + \phi\lambda^2$ for the polarization angle χ as a function of Faraday depth ϕ , we obtain

$$\begin{aligned}
P(\lambda^2) &= pI e^{2i(\chi_0 + \phi\lambda^2)} \\
&= pI e^{2i\chi_0} e^{2i\phi\lambda^2} \\
&= (pI e^{2i\chi_0}) e^{2i\phi\lambda^2} \\
&= F(\phi) e^{2i\phi\lambda^2} [\text{Jy}],
\end{aligned}$$

where $F(\phi)$ is the *Faraday dispersion function* which describes the intrinsic polarized flux as a function of Faraday depth. Since the observed polarization originates from emission along all Faraday depths, integrating this over ϕ gives the final form

$$P(\lambda^2) = \int_{-\infty}^{\infty} F(\phi) e^{2i\phi\lambda^2} d\phi [\text{Jy}].$$

Thus there is a simple expression that relates the intrinsic quantity $F(\phi)$ to the observable $P(\lambda^2)$ which takes the form of a Fourier transform. This can now be inverted to obtain the Faraday dispersion function

$$F(\phi) = \int_{-\infty}^{\infty} P(\lambda^2) e^{-2i\phi\lambda^2} d\lambda^2 [\text{rad m}^{-2}].$$

However, one is confronted with a problem: namely, that we cannot observe at wavelengths $\lambda < 0$, nor do we observe for all wavelengths $\lambda > 0$. To resolve this issue, Brentjens & de Bruyn (2005) introduce a window function $W(\lambda^2)$ which is non-zero only at wavelengths sampled by the telescope. They show that the observed polarized surface brightness can be rewritten as

$$\tilde{P}(\lambda^2) \equiv W(\lambda^2) P(\lambda^2) = W(\lambda^2) \int_{-\infty}^{\infty} F(\phi) e^{2i\phi(\lambda^2 - \lambda_0^2)} d\phi [\text{Jy}],$$

and the reconstructed Faraday dispersion function as

$$\tilde{F}(\phi) \equiv \frac{\int_{-\infty}^{\infty} \tilde{P}(\lambda^2) e^{-2i\phi(\lambda^2 - \lambda_0^2)} d\lambda^2}{\int_{-\infty}^{\infty} W(\lambda^2) d\lambda^2} = F(\phi) * R(\phi) [\text{rad m}^{-2}],$$

where $*$ denotes convolution. $\tilde{F}(\phi)$ is an approximate reconstruction of $F(\phi)$. More precisely, it is $F(\phi)$ convolved with $R(\phi)$ after Fourier filtering by the weight function $W(\lambda^2)$. $R(\phi)$ is the *rotation measure transfer function* (RMTF) which is a crucially important quantity defined by

$$R(\phi) \equiv \frac{\int_{-\infty}^{\infty} W(\lambda^2) e^{-2i\phi(\lambda^2 - \lambda_0^2)} d\lambda^2}{\int_{-\infty}^{\infty} W(\lambda^2) d\lambda^2} [\text{rad m}^{-2}],$$

which is normalized to unity at $\phi = 0$. It is a complex valued function. The real part corresponds to the response of the transform parallel to the (Q, U) vector at $\lambda_0 = \lambda$ while the imaginary part corresponds to the response orthogonal to it. Taking a look at the equations above for $\tilde{F}(\phi)$ and $R(\phi)$, these can be seen as applications of the Fourier shift theorem – since the shift theorem only affects the argument and not the absolute value of the resulting complex vector function, de-rotating these equations to $\lambda_0 \neq 0$ does not change their amplitude. The Faraday spectrum is not straightforward to interpret; in particular, there is no direct relationship between Faraday depth and physical depth. Further, the Faraday dispersion function suffers from sidelobes of the main components caused by limited coverage of the observed wavelength space. RM Synthesis is required when multiple emitting and rotating regions are located along the line of sight, as opposed to a single emitting region (i.e., Faraday screen) behind a single rotating region. RM synthesis was applied to an entire field of view for the first time by de Bruyn (1966) using pulsar observations. When applied to a complete field of view instead of just a single line of sight, the output of RM synthesis is referred to as an “RM cube”. RM synthesis is characterized by four parameters: (1) the resolution in Faraday space, which is inversely proportional to the coverage in wavelength space, (2) the maximum observable of a point-like source in Faraday space, which is inversely proportional to the width of a single frequency channel, (3) the maximum width of extended structures in Faraday space (Faraday rotating and synchrotron emitting sources), which is inversely proportional to the square of the minimum observable wavelength; wide-band observations at long wavelengths yield

high resolution in Faraday space but cannot detect extended structures, and (4) the ratio of maximum to minimum wavelengths which is crucial to recognize a range of different scales in Faraday space. Table 2 these parameters for a variety of radio telescopes. The highest resolution in Faraday space are for those with the largest wavelength coverage (LOFAR and SKA) while the largest range of scales in Faraday space are for those with the greatest ratio of maximum to minimum wavelengths (ATCA, JVLA, SKA).

Telescope	λ (m)	$\Delta\lambda^2$ (m ²)	$ \delta\phi $ (rad/m ²)	$ \Delta\phi_{\max} $ (rad/m ²)	$(\lambda_{\max}/\lambda_{\min})^2$
LOFAR highband	1.25–2.73	5.9	0.59	2.8	4.8
Westerbork (WSRT) (Netherlands)	0.17–0.23 + 0.77–0.97	0.91 ^a	3.8	110	33
GMRT (India)	0.21–0.30 + 0.47–0.52 + 0.87–0.98	0.92 ^a	3.8	71	22
DRAO, Parkes, Effelsberg (GMIMS survey)	0.17–0.23 + 0.33–1.0	0.97	3.6	110	35
Parkes (S-PASS survey)	0.12–0.14	0.004	870	220	1.4
Arecibo (GALFACTS)	0.20–0.24	0.021	165	79	1.4
JVLA (USA)	0.025–0.30	0.089	39	5,000	144
ATCA (Australia)	0.03–0.27	0.072	48	3,500	81
ASKAP (POSSUM)	0.21–0.27	0.026	130	71	1.6
SKA	0.021–6	36	0.10	7,100	82,000

^aHigh sidelobes in Faraday spectrum expected owing to the large gaps in wavelength coverage

Table 2: Spectral ranges of various radio telescopes and parameters crucial for RM synthesis. Table from Beck et al. (2012).

Rotation measure transfer function (RMTF): A crucially important quantity introduced by de Bruyn (1966) and defined by

$$R(\phi) \equiv \frac{\int_{-\infty}^{\infty} W(\lambda^2) e^{-2i\phi(\lambda^2 - \lambda_0^2)} d\lambda^2}{\int_{-\infty}^{\infty} W(\lambda^2) d\lambda^2} [\text{rad m}^{-2}],$$

which is normalized to unity at $\phi = 0$. For a simple weight function $W(\lambda^2)$ that is a top-hat (boxcar) function centered on λ_c^2 with width $\Delta\lambda^2 = \lambda_2^2 - \lambda_1^2$, the corresponding RMTF is a sinc function with a phase wind:

$$R(\phi) = e^{i\phi\lambda_c^2} \left(\frac{\sin(\phi\Delta\lambda^2)}{\phi\Delta\lambda^2} \right) [\text{rad m}^{-2}]$$

It is a complex valued function; the real part corresponds to the response of the transform parallel to the (Q, U) vector at $\lambda_0 = \lambda$ while the imaginary part corresponds to the response orthogonal to it. Ideally, the response in the entire main peak of the RMTF should be parallel to the actual polarization vector at λ_0 . Brentjens & de Bruyn (2005) show that this optimal choice of λ_0^2 is the mean of the sampled λ^2 values weighted by $W(\lambda^2)$. However, since the shift theorem of Fourier theory only applies to the argument, changing the value of λ_0 will not change the absolute value of the RMTF. A drawback of having $\lambda_0 \neq 0$ is that the polarization angle that one derives still needs to be transformed to a polarization angle at $\lambda = 0$ if one wants information on the electric or magnetic field direction of the source. In the case of a high S/N , this is easy:

$$\chi_0 = \chi(\lambda_0^2) - \phi\lambda_0^2 [\text{rad}].$$

However, if the S/N is low, the uncertainty in ϕ usually prevents accurate de-rotation to $\lambda = 0$.

Second moment: See *variance*.

Skewness: The degree of asymmetry of a distribution, and can be quantified to define the extent to which a distribution differs from a normal distribution. Skewness is defined as

$$\text{Skew}[x] = \frac{1}{N} \sum_{i=1}^N \left(\frac{x_i - \mu}{\sigma} \right)^4 - 3 [\text{dimensionless}],$$

where μ is the statistical mean and σ is the standard deviation. It can be negative, positive, zero or undefined, and like the *kurtosis*, is a dimensionless quantity.

Sonic Mach number (M_s): The ratio of the flow speed to that of the sound speed of the *interstellar medium* given by

$$M_s = \left\langle \frac{|\vec{v}|}{c_s} \right\rangle \text{ [dimensionless]},$$

where $|\vec{v}|$ is the local velocity and c_s is the sound speed. This number is a commonly used parameter of turbulence used to obtain information on gas compressibility and magnetization. Using polarization gradients of *synchrotron radiation*, it was shown by Gaensler (2011) that the turbulence of the WIM has a relatively low *sonic Mach number*, $M_s \lesssim 2$.

Spectral index (α): A measure of the dependence of radiative flux density on frequency. If flux does not follow a power-law distribution, the spectral index itself is a function of frequency. In the radio regime, a spectral index of $\alpha = 0 - 2$ indicates thermal emission while a steep negative spectrum indicates synchrotron radiation.

Scintillation:

Spectral correlation function ($S_{x,y}$): The average over all neighboring spectra of the normalized rms difference between *brightness temperatures* T_b for pairs of velocity channels (v_i, v_j) defined as

$$S_{x,y} \equiv S_{v_i, v_j} = \frac{1}{n} \sum_{a=1}^n T_b([x, y]_a, v_i) T_b([x, y]_a, v_j),$$

where n is the number of positions in the map. A histogram of $S_{x,y}$ reveals the autocorrelation properties: if $S_{x,y}$ is close to unity, the spectra do not vary much.

Starlight polarization: The polarization of initially unpolarized starlight which becomes polarized as it passes through dust grains aligned by an external magnetic field. Paramagnetic materials have unpaired electrons which, when in the presence of an external magnetic field such as the interstellar magnetic field, align in the same direction causing grain alignment. In the case of elongated dust grains, if the shortest axis is aligned with the direction of the magnetic field, then the grains will absorb light polarized along the long axis of the grain which is perpendicular to the field. This results in transmitted radiation having a polarization direction parallel to the magnetic field. Optical polarization of starlight was first imaged by Hall & Mikesell (1949) and Hiltner (1949). They found that polarized light from nearby stars had similar orientation, indicating that the polarizing mechanism was a source other than the individual stars. Shortly thereafter, Davis & Greenstein (1951) published a theory on the origin of polarized starlight. They proposed that an elongated dust grain spinning about its shortest axis would have a preferred orientation when located in a magnetic field. Starlight polarization is most useful for detecting magnetic fields in the Solar neighbourhood out to about $1 - 3$ kpc. The same large-scale alignment of spinning, aspherical dust grains that causes starlight polarization also causes *infrared polarization*.

Stellar wind bubble (SWB): A cavity light years across filled with hot gas blown into the interstellar medium by high-velocity (several thousand km s^{-1}) stellar wind from a single massive O or B star. The heliosphere blown by the Solar wind, within which all of the major planets of the Solar System are embedded, is a small example of a stellar wind bubble.

Stochastic system:

Stokes parameters:

Stokes I (I): A measure of the total intensity of radio emission.

Stokes Q (Q): A measure of the linear polarization of radio emission. The images of Stokes Q (and *Stokes U*) as well as the *linear polarized intensity* $P \equiv \sqrt{(Q^2 + U^2)}$ are often filled with complex structures that bear little resemblance to the *Stokes I* image of total intensity. The intensity variations seen in Q (as well as U and P) are the result of small-scale angular structure in the *Faraday rotation* induced by ionized gas, and are thus an indirect representation of turbulent fluctuations in the free-electron density and magnetic field throughout the *interstellar medium*.

Stokes U (U): A measure of the linear polarization of radio emission. The images of Stokes U (and *Stokes Q*) as well as the *linear polarized intensity* $P \equiv \sqrt{(Q^2 + U^2)}$ are often filled with complex structures that bear little resemblance to the *Stokes I* image of total intensity. The intensity variations seen in U (as well as Q and P) are the result of small-scale angular structure in the *Faraday rotation* induced by ionized gas, and are thus an indirect representation of turbulent fluctuations in the free-electron density and magnetic field throughout the *interstellar medium*.

Stokes V (V): A measure of circular polarization of radio emission. If $V > 0$, then the electromagnetic wave is right-handed circularly polarized (RCP), while if $V < 0$, then the electromagnetic wave is left-handed circularly polarized (LCP). Stokes V is related to the line-of-sight magnetic field in the following manner:

$$V(\nu) \propto B_{\parallel} \times \frac{dI}{d\nu} [\text{Jy}],$$

where I is *Stokes I* and ν is the observed frequency.

Striation:

Strömgren sphere: A sphere of ionized hydrogen (HII) around young OB stars.

Structure function ($S_p(\delta r)$): The structure function of order p for an observable A is given by

$$S_p(\delta r) = \langle |A(r) - A(r + \delta r)|^p \rangle,$$

for position r and position increment δr . The power-law fit to this, $S_p(\delta r) \propto \delta r^{\zeta}$, gives the slope ζ_p .

Superbubble: Also known as a *supershell*. A cavity that is hundreds of light years across filled with 1×10^6 K gas blown into the ISM by multiple SNe and stellar winds from clusters and associations of massive O and B stars. A superbubble behaves qualitatively like an individual supernova remnant, except that it has a continuous supply of energy. For the first 3 Myrs at least, their energy supply is exclusively due to stellar winds, whose cumulative power rises rapidly with time. Supernovae start exploding after $\gtrsim 3$ Myrs, and within ~ 2 Myrs, they overpower the stellar winds. From then on, the successive supernovae explosions continue to inject energy into the superbubble at a slowly decreasing rate, depending on the *initial mass function* (IMF) of the progenitor stars, until ~ 40 Myrs. Altogether, stellar winds account for a fraction comprising between $\sim 12\%$ and $\sim 17\%$ of the total energy input. The Solar System lies near the center of an old superbubble known as the *Local Bubble* whose boundary can be traced by a sudden rise in dust extinction.

Supernova: A supernova is a transient astronomical event that occurs during the last stellar evolutionary stages of a star's life, either a massive star or a white dwarf, whose destruction is marked by one final, titanic explosion. Supernovae come in two types. *Type-I* supernovae arise from old, degenerate low-mass stars which supposedly are accreting from a companion and undergoes a thermonuclear instability upon accumulation of a critical mass. *Type-II* supernovae arise from young stars with initial masses $\gtrsim 8 M_{\odot}$ whose core gravitationally collapses once it has exhausted all of its fuel. Like the bright, massive stars, Type-II supernovae are tightly confined to the spiral arms while Type-I supernovae have a more spread-out distribution similar to the general stellar population. Type-I supernovae are less frequent than their Type-II counterparts. All of them are uncorrelated in space and have basically the same repercussions on the ISM as isolated Type-II supernovae. The hot gas created by supernovae explosions (and stellar winds) in the Galactic disk rises into the halo under the influence of its own buoyancy. In the course of its upward motion, it cools down (almost adiabatically at first, then by radiative transport), and eventually condenses into cold neutral clouds. Once formed, these clouds fall ballistically towards the Galactic plane. This convective cycle of interstellar material between the disk and the halo is known as the *Galactic fountain*.

Synchrotron radiation: The radio emission produced by relativistic *cosmic rays* when accelerated radially (e.g., by magnetic fields) which is one of the most commonly used tracers of the Galactic magnetic field. Synchrotron emission has a steep spectral index of $\alpha \sim -2.75$, which results in much brighter emission at lower frequencies (this applies to both linear polarization and total intensity). For a single electron, the critical frequency of synchrotron radiation can be expressed as

$$\nu_c = \frac{3}{4\pi} \frac{q}{mc} \gamma^2 (B \sin \theta) [\text{Hz}],$$

or

$$\nu_c \sim \gamma^2 \frac{eB}{2\pi m_0} [\text{Hz}],$$

where γ is the *Lorentz factor*, e and m_0 are the charge and rest mass of the cosmic ray electron, and B is the magnetic field strength. As the cosmic ray gyrates around the local magnetic field, it generates the synchrotron radiation beamed within the shape of a cone at an angle of

$$\theta = \pm \frac{m_e c^2}{E} [\text{rad}].$$

On the surface of the cone, the radiation is 100% linearly polarized with an electric field E that has a direction of $-\mathbf{v} \times \mathbf{B}$. Synchrotron radiation from the Galaxy was the first emission detected in radio astronomy by Jansky (1933), however, it was not until the 1950's when detailed radio maps of the Galaxy were produced that the connection was made between radio emission and the synchrotron mechanism. Linear polarization of synchrotron radiation can be used to trace ordered magnetic fields in the plane of the sky (B_{\perp}). Unpolarized synchrotron emission can be indicative of a turbulent magnetic field causing depolarization via Faraday rotation of thermal electrons (synchrotron radiation cannot cause Faraday

rotation). The radiated power from an accelerating charge q with mass m by a magnetic field B at an observing frequency ν is

$$P = \frac{2}{3} \frac{q^4}{m^2 c^5} (\gamma \nu)^2 (B \sin \theta)^2 [\text{Jy}].$$

Since synchrotron radiation is proportional to the charge-to-mass ratio, electrons dominate synchrotron radiation over protons and ions by several orders of magnitude. Synchrotron radiation peaks at a characteristic frequency of

$$\nu_c = \frac{3}{4\pi} \frac{q}{mc} \gamma^2 (B \sin \theta) [\text{Hz}].$$

For radio observations with typical frequencies at or above tens of MHz and with typical magnetic field strengths of order μG , the observed population of synchrotron electrons have $\gamma \gg 1$. Synchrotron emission has a steep negative spectral index in the radio regime. Assuming that the electrons are moving isotropically, Le Roux (1961) showed that the maximum intrinsic degree of polarization (i.e., polarization fraction) of synchrotron radiation from plasma in a uniform magnetic field is a function of the electron's spectral index γ given by

$$p = \frac{3\gamma + 3}{3\gamma + 7} \text{ [dimensionless]},$$

independent of frequency and observing angle. Using observations of the Crab Nebula, Woltjer (1958) and Westfold (1959) showed that $\gamma \approx 5/3$ and therefore $p \approx 67\%$. Le Roux (1961) gives a full derivation of synchrotron radiation. Figure 5 shows the Galactic synchrotron emission at 408 MHz.

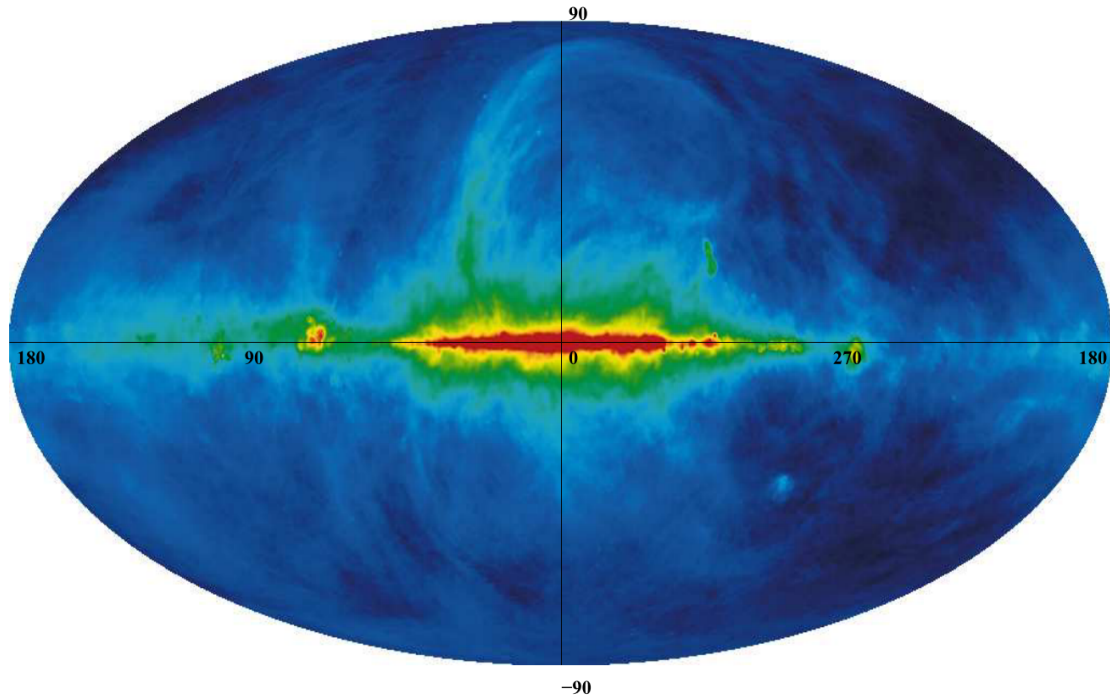


Figure 5: The synchrotron emission at 408 MHz across the entire sky in Galactic coordinates. As expected, the emission is concentrated along the Galactic plane. However, the feature known as Loop I, is clearly arching up from $\ell = 55^\circ$ towards the North Galactic Pole. This Figure is adapted from Haslam et al. (1981). Figure taken from Newton-McGee (2009).

Taylor scale:

Third moment: See *skewness*.

Toroidal magnetic field: Often the GMF is expressed in cylindrical coordinates (θ, r, z) . The *toroidal magnetic field* refers to the structures (without \vec{B}_z components) confined to a plane parallel to the Galactic plane. The toroidal fields possibly extend to the inner Galaxy, even towards the central molecular zone (CMZ).

Tsallis distribution: A function that can be fit to incremental probability distribution functions (PDFs) of turbulent density, magnetic field, and velocity. The Tsallis distribution was originally derived by Tsallis (1988) as a means to extend traditional Boltzmann-Gibbs mechanics to fractal and multifractal systems. The complex dynamics of multifractal systems apply to many natural environments, such as ISM turbulence. The Tsallis function of an arbitrary incremental PDF Δf has the form

$$R_q = a \left[1 + (q - 1) \frac{\Delta f(r)^2}{w^2} \right]^{-1/(q-1)}.$$

The fit is described by three dependent variables. The a parameter describes the amplitude while w is related to the width or dispersion of the distribution. Parameter q , referred to as the “non-extensivity parameter” or “entropic index” describes the sharpness and tail size of the distribution. The Tsallis fit parameters are in many ways similar to statistical moments. Moments, more specifically the third- and fourth-order moments, have been used to describe the density distributions and have shown sensitivities to simulation compressibility. The first- and second-order moments simply correspond to the mean and variance of a distribution. Skewness, or third-order moment, describes the asymmetry of a distribution about its mode. Skewness can have positive or negative values corresponding to right and left shifts of a distribution, respectively. The fourth-order moment, kurtosis, is a measure of a distributions peaked or flatness compared to a Gaussian distribution. Like skewness, kurtosis can have positive or negative values corresponding to increased sharpness or flatness. With regard to the Tsallis fitting parameters, the w parameter is similar to the second-order moment variance while q is closely analogous to fourth-order moment kurtosis. Unlike higher order moments, however, the Tsallis fitting parameters are dependent least-squares fit coefficients and are more sensitive to subtle changes in the PDF.

Turbulence: Astrophysical turbulence is a complex nonlinear fluid phenomenon that can occur in a multiphase medium which results in the excitation of an extreme range of correlated spatial and temporal scales. There are many injection sources on scales ranging from kp down to sub-AU. The physical processes by which kinetic energy is converted into turbulence are not well understood for the ISM. The main sources for large-scale motions are: (a) stars, whose energy input is in the form of protostellar winds, expanding HII regions, O star and Wolf-Rayet winds, supernovae, and combinations of these producing superbubbles; (b) Galactic rotation in the shocks of spiral arms or bars, in the *Balbus-Hawley instability* (also known as the magnetorotational instability), and in the gravitational scattering of cloud complexes at different epicyclic phases; (c) gaseous self-gravity through swing-amplified instabilities and cloud collapse; (d) *Kelvin-Helmholtz* and other fluid instabilities; and (e) Galactic gravity during disk-halo circulation, the *Parker instability*, and galaxy interactions. Interstellar turbulence has been characterized by *structure functions*, **correlation functions** (e.g., spatial power spectrum), *autocorrelations*, *power spectra*, *energy spectra*, and *delta variance*. Sources for small-scale turbulence observed by radio *scintillation* include sonic reflections of shock waves hitting clouds, cosmic ray streaming and other instabilities, field star motions and winds, and energy cascades from larger scales. Turbulence affects the structure and motion of nearly all temperature and density regimes of the interstellar gas. Magnetohydrodynamic (MHD) turbulence is a key element in the study of star formation, molecular cloud structure, magnetic reconnection, heat transport, and cosmic ray propagation. MHD turbulence is known to be different from a collection of linear Alfvénic waves. Does MHD turbulence, specifically the Alfvén wave modes, damp at the decoupling scale of the *ambipolar diffusion scale* L_{AD} ? Cascading rates and the anisotropy of turbulence should be accounted for carefully before a definitive conclusion about turbulent damping in the partially ionized media. Despite the importance of turbulence for ISM studies, many mysteries remain including the nature of turbulence driving and damping. The most common observational techniques for studying turbulence include scintillation studies (which are limited to fluctuations in ionized plasmas), density fluctuations via column density maps, and radio spectroscopic observations via centroids of spectral lines. Position-position-velocity (PPV) spectroscopic data have the advantage over column density maps in that it contains information on the turbulent velocity field. However, this type of data provides contributions of both velocity and density fluctuations entangled together, and the process of separating the two has proven to be a challenging problem. One of the main approaches for characterizing ISM turbulence is based on using statistical techniques and descriptions (e.g., spatial power spectrum). Although the power spectrum is useful for obtaining information about energy transfer over scales, it does not provide a full picture of turbulence, partly because it only contains information on Fourier amplitudes (i.e., two substantially different density distributions can have the same power spectrum). Probability distribution functions (PDFs) of turbulence in PPV and column density data have been studied for decades and have proven to be very useful to show that turbulence is present in the ISM, providing insight into the effects of turbulent driving and characterizing the type of turbulence in question. Many studies on turbulence focus on obtaining parameters such as *sonic and Alfvén Mach numbers*, *injection scale*, gas temperature, and *Reynolds number*. In particular, the sonic and Alfvén Mach numbers provide much coveted information on the gas compressibility and magnetization.

Turbulent fragmentation:

Turbulent magnetic field: A.k.a. “random magnetic field”. Deviations from *coherent* or *ordered* fields are taken as turbulent fields. The fluctuations of fields at scales 10 times smaller than a concerned scale are often also taken as turbulent fields.

Turbulent pressure:

Two-fluid turbulence: The turbulence of a partially ionized plasma where the ions are decoupled from the neutrals (i.e., at the scale below the *ambipolar diffusion scale*).

Type-I Supernova: Arises from old, degenerate low-mass stars which supposedly are accreting from a companion and undergoes a thermonuclear instability upon accumulation of a critical mass. Like Type-II supernovae, releases an amount of energy of $\simeq 10^{51}$ ergs.

Type-II Supernova: Arises from young stars with initial masses $\gtrsim 8 M_{\odot}$ whose core gravitationally collapses once it has exhausted all of its fuel. Like Type-I supernovae, releases an amount of energy of $\simeq 10^{51}$ ergs.

Unstable neutral medium (UNM): A thermally-unstable phase of the atomic ISM. Figure 6 shows the thermal pressure function $p(n)$. This curve has several familiar features, described in the classic paper on this subject by Field, Goldsmith & Habing (1969). These include separate branches for warm intercloud (red) and cold cloud (green) components, a maximum intercloud thermal pressure ($4400 \text{ cm}^{-3} \text{ K}$ for the curve shown), a minimum cloud thermal pressure ($1700 \text{ cm}^{-3} \text{ K}$ for this example), and a range of density ($0.8 - 7 \text{ cm}^{-3}$), or more fundamentally temperature (roughly $270 - 5500 \text{ K}$), between these two (blue) that is regarded as forbidden in equilibrium because at constant thermal pressure it is thermally unstable. In the unstable region, gas slightly above the curve is too hot for its density and cools. But at constant thermal pressure, cooling moves it to the right, to higher density, taking it further from the curve and making it cool faster, until it reaches the stable cloud branch. Similarly, gas slightly below the curve has excess heating and at constant thermal pressure moves horizontally to the left until it joins the stable intercloud component. For the standard curve, the mean midplane interstellar density in the Solar Neighbourhood (slightly over 1 cm^{-3}) is in the unstable regime. This appears to guarantee that both the cloud and intercloud branches will be populated.

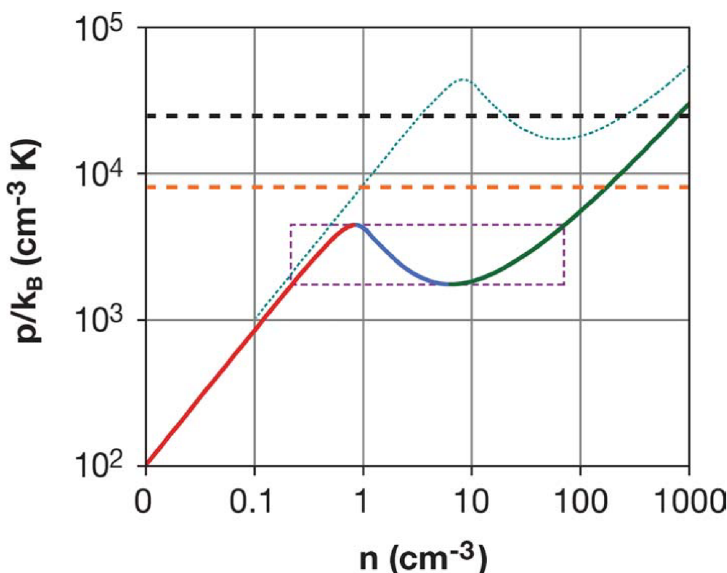


Figure 6: The Two-Phase Medium thermal pressure versus density curve is shown in the red-blue-green curve. The red segment is the thermally stable warm component, the green the corresponding stable cold component, and the blue the thermally unstable regime. The black dashed line is the total midplane pressure, the orange dashed line represents the magnetic pressure, the dashed aqua line shows how the $p(n)$ curve shifts when the heating rate is raised by a factor of 10, and the dashed purple rectangle outlines the regime of essentially zero bulk modulus. Figure taken from Cox (2005).

One of the most interesting features of $p(n)f$ is that over a density range of a factor of 350, from 0.2 to 70 cm^{-3} , the thermal pressure variation is less than a factor of three. In Figure 6, this region is shown enclosed by a dashed purple rectangle. It is a regime in which the thermal pressure offers essentially zero bulk modulus. This means that if, for some reason, the ISM had a totally random distribution of densities within this range, the corresponding distribution of thermal pressures would be observationally indistinguishable from one in which thermal pressure had an active role in arranging things, except there would be no range of forbidden densities. The small variation in thermal pressure between regions of differing density can be compensated by slight changes in the somewhat stronger magnetic field pressure. This is true when establishing pressure uniformity across the magnetic field lines, but equilibrium parallel to the field cannot be established in this way.

Volume filling factor (f): A correction factor such that a fraction f of the line of sight intersects clouds of uniform density N . There are three effects of the interstellar magnetic field that conspire to lower the filling factor of hot cavities: (1) the background magnetic pressure acting on the surrounding shells directly opposes their expansion, (2) the magnetic tension in the swept-up field lines gives rise to an inward restoring force, while the associated magnetic pressure prevents the shells from fully collapsing and, therefore, keeps them relatively thick, and (3) the enhanced external “signal speed” causes the shells to merge earlier than they would in an unmagnetized medium.

Warm ionized medium (WIM): A diffuse phase of the *interstellar medium* with a typical temperature of $T \sim 8,000\text{ K}$ and average electron density of $\sim 0.2 - 0.5\text{ cm}^{-3}$. The ionized gas has mostly been mapped using the H α line. One limitation of the H α line comes from the obscuration caused by dust, which restricts visibility to within $2 - 3\text{ kpc}$ from the Sun. Using polarization gradients of *synchrotron radiation*, it was shown by Gaensler (2011) that the turbulence of the WIM has a relatively low *sonic Mach number*, $\mathcal{M}_s \lesssim 2$.

Warm neutral medium (WNM): A thermally-stable phase of the atomic ISM with a typical density and kinetic temperature of $n \sim 0.2 - 0.9\text{ cm}^{-3}$ and $T_K \sim 5000 - 8300\text{ K}$, respectively.

Warm partially ionized medium (WPIM):

Wave turbulence:

Zeeman effect: The effect of a single spectral line splitting into multiple components in the presence of a static magnetic field due to the degeneracy between various electron energy levels that become broken when exposed to an external magnetic field. In an astrophysical context, a magnetic field produces small frequency shifts in the left- and right-handed circular polarized components of a given spectral line with respect to the intrinsic central frequency of the atom or molecule. Zeeman splitting is used to measure the parallel component of the magnetic field via atomic and molecular gas. The first measurement of an astrophysical magnetic field was using Zeeman splitting. The 21 cm line of atomic hydrogen is the most widespread, and it provides an opportunity to measure splitting in both emission and absorption. Zeeman splitting is a powerful tool as the magnetic field can be directly determined from the energy difference between the electron levels. The separation in energy of the magnetic hyperfine levels from the unsplit level of the zero magnetic field case is given by

$$\Delta E = -\mu_B m_F g B \text{ [J]},$$

where μ_B is the Bohr magneton, m_F is the quantum number of the Zeeman splitting, B is the magnetic field strength, and g is the Landé g-factor. However, the effect is difficult to observe since the frequency shift ($\Delta\nu$) in the spectral lines is small:

$$\Delta\nu = \frac{\mu_B m_F g B}{h} \text{ [Hz].}$$

Such a frequency shift is usually smaller than the spectral linewidth, making Zeeman splitting observations resolution limited. Lower frequencies produce better Zeeman splitting results because, although the splitting is independent of the line frequency itself, the higher the frequency, the broader the linewidth. The statistical sample of measured Zeeman splittings is woefully small and desperately needs to be expanded. Zeeman-splitting observations are time-consuming: typically tens of hours are required for each source. In addition, Zeeman splitting observations cannot be related to the large-scale GMF.

Zenith: The point in the sky or celestial sphere directly above an observer.

Zeroth moment:

3 Variables

Alfvén Mach number: \mathcal{M}_A [dimensionless]

Alfvén speed: v_A [m s^{-1}]

Ambipolar diffusion scale: L_{AD} [m]

Ambipolar diffusivity: ν_{AD}

Angle: θ [rad]

Autocorrelation: $C(\delta r)$ [dimensionless]

Bandwidth in frequency: $\Delta\nu$ [Hz]

Bandwidth in wavelength: $\Delta\lambda$ [Hz]

Bohr magneton: μ_B

β parameter: β

Channel central frequency: ν_c [Hz]

Channel width in frequency: $\delta\nu$ [Hz]

Channel central wavelength: λ_c [m]

Channel width in wavelength: $\delta\lambda$ [m]

Charge density: ρ_e [C m^{-3}]

Complex conjugate: $f(x)^*$ or $\bar{f}(x)$

Current density: \vec{j} [A m^{-3}]

Delta function: $\delta(x)$

Delta variance: $\sigma_{\Delta}^2(L)$

Density: ρ [m^{-3}]

Density of electrons: ρ_e [m^{-3}]

Density of ions: ρ_i [m^{-3}]

Density of neutrals: ρ_n [m^{-3}]

Diameter of window (RHT): D_W [pixels]

Dirac delta function: $\delta(x)$

Dispersion measure: DM [pc cm^{-3}]

Dynamic viscosity: μ [Pss]

Electron charge: e [C]

Electron mass: e_m [kg]

Electron plasma pressure: P_e [Pa]

Electron temperature: T_e [K]

Emission measure: EM [pc cm^{-6}]

Energy spectrum: $E(k)$ [Jy m^{-1}]

Expectation value of θ on any domain (RHT): $\langle\theta\rangle'$ [rad]

Expectation value of θ on $\theta \in [0, \pi)$ (RHT): $\langle\theta\rangle$ [rad]

Faraday depth: ϕ [rad m $^{-2}$]

Faraday dispersion function (no spectral dependence): $F(\phi)$ [rad m $^{-2}$]

Faraday dispersion function (general form): $F(\phi, \lambda)$ [rad m $^{-2}$]

Frequency: ν [Hz]

Frictional coupling coefficient between ions and neutrals: α [dimensionless]

FWHM of RMTF main peak: $\Delta\phi$ [rad m $^{-2}$]

Fourier transform (FT): $\hat{f}(x)$

Incremental position: δr [m]

Intensity threshold: Z [dimensionless]

Jansky: Jy [unit]

Joule: J [unit]

Diameter of kernel (RHT): D_K [pixels]

Landé g-factor: g

Lorentz factor: γ [dimensionless]

Mach number: \mathcal{M} [dimensionless]

Magnetic field: \vec{B} [μG]

Mean: $\mu(x)$

Momentum diffusivity: ν [$\text{m}^2 \text{s}^{-1}$]

Number density: n [m^{-3}]

Number of θ bins (RHT): n [dimensionless]

Order: p [dimensionless]

Planck constant: h [J s]

Planck constant (reduced): \hbar [J s]

Polarization angle: χ [rad]

- Polarization angle (RHT):** χ_{RHT} [rad]
Polarization angle at $\lambda = 0$: χ_0 [rad]
Polarization fraction: $p(\lambda^2)$ [dimensionless]
Polarization gradient: $\left| \frac{\partial \vec{P}}{\partial s} \right|$ or $|\vec{\nabla} \vec{P}|$ [Jy beam $^{-1}$]
Polarization gradient (maximum value): $\left| \frac{\partial \vec{P}}{\partial s} \right|_{\max}$ or $|\vec{\nabla} \vec{P}|_{\max}$ [Jy beam $^{-1}$]
Polarization gradient (radial component; maximum value): $\left| \frac{\partial \vec{P}}{\partial s} \right|_{\text{rad}}$ [Jy beam $^{-1}$]
Polarization gradient (tangential component; maximum value): $\left| \frac{\partial \vec{P}}{\partial s} \right|_{\tan}$ [Jy beam $^{-1}$]
Polarization gradient (direction): $\arg(\vec{\nabla} \vec{P})$ [rad]
Polarized intensity: P [Jy]
Polarized surface brightness: $P(\lambda^2)$ [Jy]
Polarized surface brightness (observed): $\tilde{P}(\lambda^2)$ [Jy]
Position: r [m]
Power spectrum: $P(k)$
Quantum number of Zeeman splitting: m_F
Radial component of polarization gradient: $\frac{\partial \mathbf{P}}{\partial s_{\text{rad}}}$ [Jy pc $^{-1}$]
Resistivity: η [Ω m]
Rest mass: m_0 [kg]
Reynolds number: Re [dimensionless]
Reynolds number for ambipolar diffusion: R_{AD} [dimensionless]
RHT angle: θ [rad]
RHT backprojection: $R(x, y)$ [dimensionless]
RHT backprojection sampling disk around star: $R_*(x, y)$ [dimensionless]
RHT distance: ρ [pixels]
RHT intensity vs angle: $R(\theta, x_0, y_0)$ [dimensionless]
Rotation measure: RM [rad m $^{-2}$]
Rotation measure transfer function (RMTF): $R(\phi)$ [rad m $^{-2}$]
Sonic Mach number: M_s [dimensionless]
Sound speed: c_s [m s $^{-1}$]
Specific heat: c_p [J kg $^{-1}$ K]
Spectral correlation function: $S_{x,y}$ [dimensionless]
Spectral index: α [dimensionless]
Speed of light: c [m s $^{-1}$]
Standard deviation: $\sigma(x)$
Stokes I: I [Jy]
Stokes Q: Q [Jy]
Stokes Q (RHT): Q_{RHT} [Jy]
Stokes U: U [Jy]
Stokes U (RHT): U_{RHT} [Jy]
Stokes V: V [Jy]
Structure function: S_p
Structure function power-law slope: ζ_p
Tangential component of polarization gradient: $\frac{\partial \mathbf{P}}{\partial s_{\tan}}$ [Jy pc $^{-1}$]
Thermal conductivity: k [W m $^{-1}$ K]
Thermal diffusivity: α [m 2 s $^{-1}$]
Variance: σ^2
Velocity: \vec{v} [m s $^{-1}$]
Viscosity coefficient: μ [Pas]
Wavelength: λ [m]
Wavelength to which all polarization vectors are de-rotated: λ_0 [m]
Wavenumber: k [m $^{-1}$]
Weight function: $W(\lambda^2)$ [dimensionless]
Zeeman splitting energy difference: ΔE [J]

Zeeman splitting frequency difference: $\Delta\nu$ [Hz]

4 Equations

Alfvén Mach number:

$$\mathcal{M}_A = \left\langle \frac{|\vec{v}|}{v_A} \right\rangle \text{ [dimensionless]}$$

Alfvén speed:

$$v_A = \frac{|\vec{B}|}{\sqrt{\rho}} \text{ [m s}^{-1}\text{]}$$

Ambipolar diffusion scale:

$$L_{AD} = \frac{V_A}{\alpha \rho_i} \text{ [m]}$$

Ambipolar diffusivity:

$$\nu_{AD} = \frac{B^2}{4\pi \rho_i \rho_n \alpha} \text{ [m}^2 \text{s}^{-1}\text{]}$$

Autocorrelation:

$$C(\delta r) = \langle f(r)f(r + \delta r) \rangle \text{ [dimensionless]}$$

β parameter:

$$\beta \equiv \frac{c_s^2}{v_A^2} \text{ [dimensionless]}$$

Channel central wavelength:

$$\lambda_c^2 \approx \frac{c^2}{\nu_c^2} \left(1 + \frac{3}{4} \left(\frac{\delta\nu}{\nu_c} \right)^2 \right) \text{ [m}^2\text{]}$$

(Brentjens & de Bruyn, 2005)

Charge conservation:

$$\frac{\partial \rho_e}{\partial t} + \vec{\nabla} \cdot \vec{j} = 0$$

Channel width in wavelength:

$$\delta\lambda^2 \approx \frac{2c^2\delta\nu}{\nu_c^3} \left(1 + \frac{1}{2} \left(\frac{\delta\nu}{\nu_c} \right)^2 \right) \text{ [m}^2\text{]}$$

(Brentjens & de Bruyn, 2005)

Current density:

$$\vec{j} = c \nabla \times \frac{\vec{B}}{4\pi} \text{ [A m}^{-2}\text{]}$$

(Schoeffler et al., 2016)

Delta variance:

$$\sigma_\Delta^2(L) = \left\langle \int_0^{3L/2} (A[r+x] - \langle A \rangle) \odot (x)^2 dx \right\rangle,$$

Dispersion measure (DM):

$$DM = - \int_{\text{source}}^{\text{observer}} n_e d\ell \text{ [pc cm}^{-3}\text{]}$$

Electron plasma pressure:

$$P_e = T_e \eta \text{ [Pa]}$$

(Schoeffler et al., 2016)

Electron temperature:

$$T_e = \frac{P_e}{\eta} \text{ [K]}$$

(Schoeffler et al., 2016)

Emission measure:

$$EM = - \int_{\text{source}}^{\text{observer}} n_e^2 d\ell \text{ [pc cm}^{-6}\text{]}$$

Expectation value of θ on any domain (RHT):

$$\langle \theta \rangle' = \frac{1}{2} \arctan \left[\frac{\int \sin(2\theta) R_*(\theta) d\theta}{\int \cos(2\theta) R_*(\theta) d\theta} \right]$$

Expectation value of θ on $\theta \in [0, \pi]$ (RHT):

$$\langle \theta \rangle = \pi - \text{mod}(\langle \theta \rangle' + \pi, \pi) \text{ [rad]}$$

Faraday depth:

$$\phi(\vec{r}) = -0.81 \int_{\text{source}}^{\text{observer}} n_e \vec{B} \cdot d\vec{r} [\text{rad m}^{-2}]$$

Faraday depth standard error:

$$\begin{aligned} \sigma_\phi &= \left[\frac{1}{N-2} \frac{\sum_i \chi_i^2}{\sum_i (\lambda_i^2)^2 - N^{-1} (\sum_i \lambda_i^2)^2} \right]^{-1} \\ &= \left[\frac{1}{N-2} \frac{(N-1)(\sigma_\chi^2 + \langle \chi \rangle)}{\sum_i (\lambda_i^2)^2 - N^{-1} (\sum_i \lambda_i^2)^2} \right]^{-1} \\ &= \left[\frac{N-1}{N-2} \frac{\sigma_\chi^2}{\sum_i (\lambda_i^2)^2 - N^{-1} (\sum_i \lambda_i^2)^2} \right]^{-1} \\ &\approx \left[\frac{\sigma_Q^2 \approx \sigma_U^2 \approx \sigma^2}{4(N-2) \|P\|^2 \sigma_{\lambda^2}^2} \right]^{-1} [\text{rad m}^{-2}] \end{aligned}$$

(Brentjens & de Bruyn, 2005)

Faraday dispersion function:

$$F(\phi) = \int_{-\infty}^{\infty} P(\lambda^2) e^{-2i\phi\lambda^2} d\lambda^2 [\text{rad m}^{-2}]$$

Faraday dispersion function (reconstructed):

$$\tilde{F}(\phi) \equiv \frac{\int_{-\infty}^{\infty} \tilde{P}(\lambda^2) e^{-2i\phi(\lambda^2 - \lambda_0^2)} d\lambda^2}{\int_{-\infty}^{\infty} W(\lambda^2) d\lambda^2} = F(\phi) * R(\phi) [\text{rad m}^{-2}]$$

Fourier transform (FT):

$$\hat{f}(x) = \int_{-\infty}^{\infty} f(x') e^{-2\pi x x'} dx'$$

Induction equation:

$$\frac{\partial \vec{B}}{\partial t} = \nabla \times (\vec{v} \times \vec{B}) + \frac{\eta c^2}{4\pi} \nabla^2 \vec{B} - \frac{1}{en} \nabla \times (\vec{j} \times \vec{B}) - \frac{c}{ne} \nabla n \times \nabla T_e$$

(Schoeffler et al., 2016)

Inverse Fourier transform (FT):

$$f(x) = \int_{-\infty}^{\infty} \hat{f}(x') e^{2\pi i x x'} dx'$$

Kurtosis:

$$\text{Kurt}[x] = \frac{1}{N} \sum_{i=1}^N \left(\frac{x_i - \mu}{\sigma} \right)^3 [\text{dimensionless}]$$

Lorentz factor:

$$\gamma = \sqrt{\frac{1 - (v/c)^2}{c^2}} [\text{dimensionless}]$$

Magnetohydrodynamic (MHD) equations:

$$\begin{aligned} \vec{\nabla} \cdot \vec{B} &= 0 \\ \vec{\nabla} \cdot \vec{E} &= 4\pi\rho_e \\ c\vec{\nabla} \times \vec{E} &= -\frac{\partial \vec{B}}{\partial t} \\ c\vec{\nabla} \times \vec{B} &= 4\pi\vec{j} + \frac{\partial \vec{E}}{\partial t} \end{aligned}$$

Number of θ bins (RHT):

$$n_\theta = \left[\pi \frac{\sqrt{2}}{2} (D_W - 1) \right] [\text{dimensionless}]$$

Polarization angle:

$$\begin{aligned}\chi &= \frac{1}{2} \arctan \left(\frac{U}{Q} \right) [\text{rad}] \\ &= \chi_0 + \text{RM} \lambda^2 [\text{rad}]\end{aligned}$$

Polarization angle (RHT):

$$\chi_{\text{RHT}} = \frac{1}{2} \arctan \left(\frac{U_{\text{RHT}}}{Q_{\text{RHT}}} \right) [\text{rad}]$$

Polarization angle distribution standard error:

$$\sigma_\chi = \left[\frac{1}{N-1} \sum_i \chi_i^2 - \langle \chi \rangle \right]^{-1} [\text{rad}]$$

(Brentjens & de Bruyn, 2005)

Polarization angle standard error:

$$\begin{aligned}\sigma_\chi &= \sqrt{\left(\frac{\partial \chi}{\partial Q} \right)^2 \sigma_Q^2 + \left(\frac{\partial \chi}{\partial U} \right)^2 \sigma_U^2} \\ &= \sqrt{\left(\frac{\partial \frac{1}{2} \arctan \frac{U}{Q}}{\partial Q} \right)^2 \sigma_Q^2 + \left(\frac{\partial \frac{1}{2} \arctan \frac{U}{Q}}{\partial U} \right)^2 \sigma_U^2} \\ &= \sqrt{\left(\frac{1}{4} \frac{U^2}{(Q^2 + U^2)^2} \right) \sigma_Q^2 + \left(\frac{1}{4} \frac{Q^2}{(Q^2 + U^2)^2} \right) \sigma_U^2} \\ &= \frac{U^2 \sigma_Q^2 + Q^2 \sigma_U^2}{4 \|P\|^4} [\text{rad}]\end{aligned}$$

(Brentjens & de Bruyn, 2005)

Polarization angle at $\lambda = 0$ standard error:

$$\sigma_{\chi_0} = \left[\frac{\sigma_Q^2 \approx \sigma_U^2 \approx \sigma^2}{4(N-2)\|P\|^2} \left(\frac{N-1}{N} + \frac{\lambda_0^4}{\sigma_{\lambda^2}^2} \right) \right]^{-1} [\text{rad}]$$

(Brentjens & de Bruyn, 2005)

Polarization gradient:

$$\left| \frac{\partial \vec{P}}{\partial s} \right| = \sqrt{\cos^2 \theta \left(\left(\frac{\partial Q}{\partial x} \right)^2 + \left(\frac{\partial U}{\partial x} \right)^2 \right) + 2 \cos \theta \sin \theta \left(\frac{\partial Q}{\partial x} \frac{\partial Q}{\partial y} + \frac{\partial U}{\partial x} \frac{\partial U}{\partial y} \right) + \sin^2 \theta \left(\left(\frac{\partial Q}{\partial y} \right)^2 + \left(\frac{\partial U}{\partial y} \right)^2 \right)} [\text{Jy beam}^{-1}]$$

(Herron, 2005)

Polarization gradient (direction):

$$\arg(\vec{\nabla} \vec{P}) \equiv \arctan \left[\text{sign} \left(\frac{\partial Q}{\partial x} \frac{\partial Q}{\partial y} + \frac{\partial U}{\partial x} \frac{\partial U}{\partial y} \right) \frac{\sqrt{\left(\frac{\partial Q}{\partial y} \right)^2 + \left(\frac{\partial U}{\partial y} \right)^2}}{\sqrt{\left(\frac{\partial Q}{\partial x} \right)^2 + \left(\frac{\partial U}{\partial x} \right)^2}} \right] [\text{rad}]$$

(Herron, 2005)

Polarization gradient (maximum value):

$$\left| \frac{\partial \vec{P}}{\partial s} \right|_{\max} = \sqrt{\frac{1}{2} \left[\left(\frac{\partial Q}{\partial x} \right)^2 + \left(\frac{\partial U}{\partial x} \right)^2 + \left(\frac{\partial U}{\partial x} \right)^2 + \left(\frac{\partial U}{\partial y} \right)^2 \right] + \frac{1}{2} \sqrt{\left[\left(\frac{\partial Q}{\partial x} \right)^2 + \left(\frac{\partial U}{\partial x} \right)^2 + \left(\frac{\partial U}{\partial x} \right)^2 + \left(\frac{\partial U}{\partial y} \right)^2 \right]^2 - 4 \left[\frac{\partial Q}{\partial x} \frac{\partial U}{\partial y} - \frac{\partial Q}{\partial y} \frac{\partial U}{\partial x} \right]^2}}$$

(Herron, 2005)

Polarization gradient (radial component):

$$\left| \frac{\partial \vec{P}}{\partial s} \right|_{\text{rad}} = \cos \left(\arctan \frac{U}{Q} \right) \left(\frac{\partial Q}{\partial x} \cos \theta + \frac{\partial Q}{\partial y} \sin \theta \right) + \sin \left(\arctan \frac{U}{Q} \right) \left(\frac{\partial U}{\partial x} \cos \theta + \frac{\partial U}{\partial y} \sin \theta \right) [\text{Jy beam}^{-1}]$$

(Herron, 2005)

Polarization gradient (radial component; maximum value):

$$\left| \frac{\partial \vec{P}}{\partial s} \right|_{\text{rad}, \max} = \sqrt{\frac{\left(Q \frac{\partial Q}{\partial x} + U \frac{\partial U}{\partial x} \right)^2 + \left(Q \frac{\partial Q}{\partial y} + U \frac{\partial U}{\partial y} \right)^2}{Q^2 + U^2}} [\text{Jy beam}^{-1}]$$

(Herron, 2005)

Polarization gradient (tangential component):

$$\left| \frac{\partial \vec{P}}{\partial s} \right|_{\tan} = -\sin \left(\arctan \frac{U}{Q} \right) \left(\frac{\partial Q}{\partial x} \cos \theta + \frac{\partial Q}{\partial y} \sin \theta \right) + \cos \left(\arctan \frac{U}{Q} \right) \left(\frac{\partial U}{\partial x} \cos \theta + \frac{\partial U}{\partial y} \sin \theta \right) [\text{Jy beam}^{-1}]$$

(Herron, 2005)

Polarization gradient (tangential component; maximum value):

$$\left| \frac{\partial \vec{P}}{\partial s} \right|_{\tan, \max} = \sqrt{\frac{\left(Q \frac{\partial U}{\partial x} - U \frac{\partial Q}{\partial x} \right)^2 + \left(Q \frac{\partial U}{\partial y} - U \frac{\partial Q}{\partial y} \right)^2}{Q^2 + U^2}} [\text{Jy beam}^{-1}]$$

(Herron, 2005)

Polarization fraction:

$$p(\lambda^2) = \frac{P(\lambda^2)}{I(\lambda^2)} \text{ [dimensionless]}$$

Polarized intensity:

$$P \equiv \sqrt{Q^2 + U^2} \text{ [Jy]}$$

Polarized intensity standard error:

$$\begin{aligned} \sigma_P &= \sqrt{\left(\frac{\partial ||P||}{\partial Q} \right)^2 \sigma_Q^2 + \left(\frac{\partial ||P||}{\partial U} \right)^2 \sigma_U^2} \\ &= \sqrt{\left(\frac{Q^2}{Q^2 + U^2} \right) \sigma_Q^2 + \left(\frac{U^2}{Q^2 + U^2} \right) \sigma_U^2} \\ &= \sqrt{\frac{Q^2}{||P||^2} \sigma_Q^2 + \frac{U^2}{||P||^2} \sigma_U^2} \text{ [Jy]} \end{aligned}$$

(Brentjens & de Bruyn, 2005)

Polarized surface brightness:

$$\begin{aligned} P(\lambda^2) &= ||p(\lambda^2)|| I e^{2i\chi} = p(\lambda^2) I(\lambda^2) = Q + iU \text{ [Jy]} \\ &= \int_{-\infty}^{\infty} F(\phi) e^{2i\phi\lambda^2} d\phi \text{ [Jy]} \end{aligned}$$

Polarized surface brightness (absolute):

$$||P(\lambda^2)|| = \sqrt{Q^2 + U^2} \text{ [Jy]}$$

Polarized surface brightness (observed):

$$\tilde{P}(\lambda^2) \equiv W(\lambda^2) P(\lambda^2) = W(\lambda^2) \int_{-\infty}^{\infty} F(\phi) e^{2i\phi(\lambda^2 - \lambda_0^2)} d\phi \text{ [Jy]}$$

Power spectrum:

$$P(k) = \hat{f}(k) \hat{f}(k)^*$$

Reynolds number:

$$\text{Re} = \frac{\rho v L}{\mu} \text{ [dimensionless]},$$

Reynolds number for ambipolar diffusion:

$$\text{R}_{\text{AD}} = \frac{LV}{\nu_{\text{AD}}} \text{ [dimensionless]}$$

RHT backprojection:

$$R(x, y) = \int R(\theta, x, y) d\theta \text{ [dimensionless]}$$

RHT backprojection sampling disk around star:

$$R_*(x, y) = \iint_{\text{disk}} R(\theta, x, y) dx dy \text{ [dimensionless]}$$

RHT distance:

$$\rho = x \cos \theta + y \sin \theta \text{ [pixels]}$$

Rotation measure:

$$\text{RM} = \frac{d\chi(\lambda^2)}{d\lambda^2} \text{ [rad m}^{-2}\text{]}$$

$$\text{RM} = -0.81 \int_{\text{source}}^{\text{observer}} n_e \vec{B} \cdot \vec{dl} \text{ [rad m}^{-2}\text{]}$$

Rotation measure transfer function (RMTF):

$$R(\phi) \equiv \frac{\int_{-\infty}^{\infty} W(\lambda^2) e^{-2i\phi(\lambda^2 - \lambda_0^2)} d\lambda^2}{\int_{-\infty}^{\infty} W(\lambda^2) d\lambda^2} [\text{rad m}^{-2}]$$

Rotation measure transfer function (RMTF) for box-car weight function $W(\lambda^2)$:

$$R(\phi) = e^{i\phi\lambda_c^2} \left(\frac{\sin(\phi\Delta\lambda^2)}{\phi\Delta\lambda^2} \right) [\text{rad m}^{-2}]$$

Skewness:

$$\text{Skew}[x] = \frac{1}{N} \sum_{i=1}^N \left(\frac{x_i - \mu}{\sigma} \right)^4 - 3 \text{ [dimensionless]}$$

Sonic Mach number:

$$\mathcal{M}_s = \left\langle \frac{|\vec{v}|}{c_s} \right\rangle \text{ [dimensionless]}$$

Spectral correlation function:

$$S_{x,y} \equiv S_{v_i, v_j} = \frac{1}{n} \sum_{a=1}^n T([x, y]_a, v_i) T([x, y]_a, v_j)$$

Stokes Q (RHT):

$$Q_{\text{RHT}} = \int \cos(2\theta) R(\theta) d\theta \text{ [Jy]}$$

Stokes Q (RHT):

$$U_{\text{RHT}} = \int \sin(2\theta) R(\theta) d\theta \text{ [Jy]}$$

Stokes V magnetic field:

$$V(\nu) \propto B_{\parallel} \times \frac{dI}{d\nu} \text{ [Jy]}$$

Structure function:

$$S_p(\delta r) = \langle |A(r) - A(r + \delta r)|^p \rangle,$$

Synchrotron radiation angle:

$$\theta = \pm \frac{m_c c^2}{E} \text{ [rad]}$$

Synchrotron radiation characteristic frequency:

$$\nu_c = \frac{3}{4\pi} \frac{q}{mc} \gamma^2 (B \sin \theta) \text{ [Hz]}$$

$$\nu_c \sim \gamma^2 \frac{eB}{2\pi m_0} \text{ [Hz]}$$

Synchrotron radiation maximum polarization:

$$p = \frac{3\gamma + 3}{3\gamma + 7} \text{ [dimensionless]}$$

Synchrotron radiation power:

$$P = \frac{2}{3} \frac{q^4}{m^2 c^5} (\gamma \nu)^2 (B \sin \theta)^2 \text{ [Jy]}$$

Wavelength squared distribution standard error:

$$\sigma_{\lambda^2} = \left[\frac{1}{N-1} \left(\sum_i \lambda_i^4 - N^{-1} (\sum_i \lambda_i^2)^2 \right) \right]^{-1} \text{ [m}^{-2}\text{]}$$

Zeeman splitting energy difference:

$$\Delta E = -\mu_B m_F g B \text{ [J]}$$

Zeeman splitting frequency difference:

$$\Delta\nu = \frac{\mu_B m_F g B}{h} \text{ [Hz]}$$